

**PREPARATION AND APPLICATION OF ZnO/MULLITE FOR THE
INACTIVATION OF *ESCHERICHIA COLI* AND *SALMONELLA ENTERICA* IN
WATER**

By

**ANTHONY DAUDA JOSEPH B.Eng, PGD (A.B.U) MNSE
(MSc/Eng/45453/2012-2013)**

**DEPARTMENT OF CHEMICAL ENGINEERING,
FACULTY OF ENGINEERING,
AHMADU BELLO UNIVERSITY, ZARIA
NIGERIA.**

MAY, 2016

**PREPARATION AND APPLICATION OF ZnO/MULLITE FOR THE
INACTIVATION OF *ESCHERICHIA COLI* AND *SALMONELLA ENTERICA* IN
WATER**

By

**ANTHONY DAUDA JOSEPH B.Eng, PGD (A.B.U) MNSE
(MSc/Eng/45453/2012-2013)**

**A DISSERTATION SUBMITTED TO THE SCHOOL OF POSTGRADUATE STUDIES,
AHMADU BELLO UNIVERSITY, ZARIA.**

**IN PARTIAL FULFILLMENT OF THE REQUIREMENTS FOR THE AWARD OF
A MASTER OF SCIENCE DEGREE IN CHEMICAL ENGINEERING.**

**DEPARTMENT OF CHEMICAL ENGINEERING,
FACULTY OF ENGINEERING,
AHMADU BELLO UNIVERSITY, ZARIA
NIGERIA.**

MAY, 2016

DECLARATION

I declare that the work in this dissertation titled “PREPARATION AND APPLICATION OF ZnO/MULLITE FOR THE INACTIVATION OF *ESCHERICHIA COLI* AND *SALMONELLA ENTERICA* IN WATER” was carried out by me in the Department of Chemical Engineering, Ahmadu Bello University, Zaria, under the supervision of Dr. Abdulhamid Hamza and Dr. O.A AJAYI of the Department of Chemical Engineering, Ahmadu Bello University, Zaria. The information derived from the literature has been duly acknowledged in the text and a list of reference provided. No part of this dissertation was previously presented for another degree in this University or any other Institution.

Signature

Date

CERTIFICATION

This dissertation entitled “**PREPARATION AND APPLICATION OF ZnO/MULLITE FOR THE INACTIVATION OF *ESCHERICHIA COLI* AND *SALMONELLA ENTERICA* IN WATER**” by Anthony Dauda JOSEPH, meets the regulations governing the award of the degree of Master of Science (M.Sc) of the Ahmadu Bello University, and is approved for its contribution to knowledge and literary presentation.

Dr. Abdulhamid Hamza
Chairman, Supervisory Committee

Date

Dr. O.A Ajayi
Member, Supervisory Committee

Date

Dr. S.M. Waziri
Head, Dept. of Chemical Engineering

Date

Prof. Kabir Bala
Dean, School of Postgraduate Studies

Date

DEDICATION

This M.Sc dissertation is dedicated to my beloved wife and son.

ACKNOWLEDGEMENTS

All praises, glory and adorations to the Almighty God, the creator of the universe. To Him alone belong all attributes of perfection. I am indeed thankful for the gift of life and for making this research work a reality.

My deepest appreciation goes to my supervisor, Dr. Abdulhamid Hamza, for his effort and support in guiding me throughout my MSc research. Your magnanimous sea of knowledge has being the aid to the realization of this work. I would also like to express heartfelt thanks to my co-supervisor, Dr. O.A Ajayi for giving me guidance and opinions to improve my research. God will continue to bless you sir. My heartfelt appreciation goes to both academic and non-academic staff of the Department of Chemical Engineering, Ahmadu Bello University, Zaira for their constructive criticism and technical inputs that made this research a success.

To all my friends and colleagues: Madam Shola, Gold, Toba, Zanna, Kate, Gbenga, Tomilola, Moshood, Abdul, Bugaje, Mukhtar, Mr. Y, Abudraulf, Zikira and those I forget to mention their names, thank you all for your contributions to the success of this work. I also wish to acknowledge the immense courage and invaluable support of my parents (especially my late daddy who was there at the beginning of this work) in making my pursuit of education a reality. Indeed, I will always live to remember and gratify your role in my life. I sincerely render my appreciation to all my family members for their prayers, encouragement and special support throughout my educational pursuits. Finally I cannot forget the rare supportive roles of my darling wife and my lovely kid, without your supports this noble course could not have been accomplished. Once again, thank you all.

ABSTRACT

Several procedures are commonly used for water disinfection from bacteria. Unfortunately each procedure has its shortcomings. The most important shortcoming is the formation of disinfection by-products. Photodegradation of microorganisms using photocatalysts (such as ZnO) could be a good alternative. However, ZnO is a wide band gap (3.2 eV) semiconductor, and demands UV irradiations for excitation. In order to make the synthesized ZnO active under visible light for the photo excitation, the ZnO must be supported. In this work, ZnO semiconductor particles, supported with mullite in varied proportion was developed (10%-ZnO/mullite, 20%-ZnO/mullite, 30%-ZnO/mullite, 40%-ZnO/mullite and 50%-ZnO/mullite) and synthesized by impregnation method followed by calcination at 1200 °C. Different concentrations (0.5g/L, 1g/L, 1.5g/L and 2g/L) of the synthesized photocatalyst were used to disinfect water and also to reduce the COD level under visible light irradiation. Between 90%-98% inactivation of *E.coli* and *S.enterica* and 64% COD reduction was achieved in 90 minutes respectively under visible light irradiation. The 1g/L and 30%-ZnO/mullite photocatalyst gave the best bacteria inactivation of 98% while the 1g/L and 50%-ZnO/mullite photocatalyst gave the highest percentage COD reduction of 64. Control experiments that were carried out showed 35% inactivation and 14% COD reduction under visible light irradiation. The synthesized photocatalyst were characterized using UV-Visible absorption spectrophotometry, X-ray diffraction (XRD), Specific surface area analysis, pH of point of zero charge (pH_{PZC}) analyses and Scanning electron microscopy (SEM) techniques. The kinetics of the degradation of methylene blue (MB) carried out under visible light irradiation using the synthesized photocatalyst, gave a degradation percentages of 82 for the unsupported ZnO and 68 for the 50%-ZnO/mullite.

TABLE OF CONTENTS

Content	page
Title page	ii
Declaration	iii
Certification	iv
Dedication	v
Acknowledgements	vi
Abstract	vii
Table of contents	viii
List of Tables	xiii
List of Figures	xiv
List of Plates	xvi
List of Appendix	xvii
List of Abbreviations	xviii
CHAPTER ONE	
1.0 INTRODUCTION	1
1.1 Preamble	1
1.2 Problem Statement	3
1.3 Aim and Objectives	3
1.4 Justification	4
1.5 Scope of the Work	4

CHAPTER TWO

2.0	LITERATURE REVIEW	5
2.1	Photocatalysis	5
2.2	Types of Photocatalysis	5
2.2.1	Homogeneous photocatalysis	5
2.2.2	Heterogeneous photocatalysis	7
2.3	Mechanism and Fundamentals of Photocatalytic Reactions	8
2.4	Types of Photocatalysts and their Characteristics	9
2.5	Radiation Sources for Photocatalysis	10
2.6	Factors Affecting the Degradation Performance	11
2.6.1	Catalyst loading	11
2.6.2	pH of the solution	11
2.6.3	Size and structure of the photocatalyst	14
2.6.4	Reaction temperature	14
2.6.5	Concentration and nature of pollutants	15
2.6.6	Surface area	15
2.6.7	Recombination	16
2.7	Methods of Improving the Activity of Photocatalyst	17
2.7.1	Sensitization	17
2.7.2	Doping	18
2.8	Particle Size	19
2.9	Photocatalytic Degradation Kinetics	20
2.10	Characterization of Photocatalysts	21

2.10.1 X-ray diffraction (XRD) spectroscopy	21
2.10.2 X-ray florescence (XRF) spectroscopy	21
2.10.3 X-ray photoelectron spectroscopy	22
2.10.4 UV-Vis absorption	22
2.10.5 Brunauer-Emmett-Teller (BET)	23
2.11 Kaolinite	23
2.11.1 Structural transformations of kaolinite	24
2.12 Mullite	25
2.13 Zinc Oxide	26
2.14 Water Disinfection	27
2.14.1 Disinfection by oxidation processes	27
2.15 Disinfection Mechanisms	30
2.16 Microorganisms	31
2.16.1 Types of pathogenic microorganisms	32
2.16.2 Bacteria	32
2.16.3 <i>Escherichia coli</i> (<i>E.coli</i>)	32
2.16.4 <i>Salmonella enterica</i>	33
2.17 Some Previous Related Works	33
CHAPTER THREE	
3.0 MATERIALS AND METHODS	36
3.1 Materials	36
3.2 Wet Beneficiation of Kankara Kaolin Clay	39
3.3 Preparation of ZnO/ Mullite Photocatalyst	39

3.4	Characterization of the Synthesized ZnO/ Mullite Support.	40
3.4.1	Determination of point of zero charge (pH_{pzc})	40
3.4.2	Specific surface area determination (Sear's method)	41
3.5	Photocatalytic Degradation of Methylene Blue	41
3.6	Preparation of Bacterial Cultures	42
3.7	Bacterial Photo-Inactivation Experiments	43
3.7.1	Measuring the remaining concentration of bacteria	43
3.8	Measurement of COD	44
3.8.1	Measurement of pH	44
3.8.2	Measurement of conductivity	44
3.8.3	Measurement of TDS	45
3.9	X-RAY Spectrometry	45
3.9.1	Sample Preparation	45
3.9.2	Procedure of the analysis	45
3.10	X-Ray Diffraction	46
3.11	Scanning Electron Microscopy	47
CHAPTER FOUR		
RESULTS AND DISCUSSION		48
4.1.	Characterization of the synthesized photocatalysts	48
4.1.1.	Chemical compositions of raw kaolin, beneficiated kaolin and mullite	48
4.1.2	XRD analysis of the synthesized photocatalysts	50
4.1.3	Scanning electron microscopy (SEM) analyses	52

4.1.4.	Specific surface areas of the synthesized photocatalysts	54
4.1.5.	pH at point of zero charge of the photocatalyst	55
4.1.6	Preliminary evaluation of photocatalytic activity of the synthesized ZnO and ZnO/mullite composites.	56
4.2	Photocatalytic inactivation of <i>E.coli</i> and <i>S.entericain</i> water	60
4.2.1	Effect of photocatalyst concentration on efficiency	62
4.2.2	Effect of control experiments on bacterial inactivation	67
4.2.3	Effect of bacteria concentration on photocatalyst efficiency	68
4.2.4	Photocatalytic treatment of Zaria dam raw water.	68
4.3.	Kinetic Study for <i>E.coli</i> Inactivation and Microbicidal Photonic Efficiency	70
CHAPTER FIVE		
CONCLUSIONS AND RECOMMENDATIONS		72
Conclusions		72
Recommendation		73
REFERENCES		74
APPENDICES		81

LIST OF TABLES

Table 2.1.	Band gap energies of various semiconductors at relevant wavelengths	10
Table 2.2.	Optimum dosage of photocatalyst for degradation of organic compounds	13
Table 2.3	Comparison of the Main Water Disinfectants	29
Table 3.1.	List of equipment used and their specifications	37
Table 3.2:	Amount of ZnCO ₃ mixed with kaolinite clay for photocatalyst preparation.	40
Table 4.1:	Chemical compositions of the Kankara kaolin, beneficiated kaolin and mullite	49
Table 4.2	Specific surface areas of the synthesized ZnO and various ratios of ZnO/Mullite	55
Table 4.3.	pH at zero of point charge of the photocatalysts	56
Table 4.4:	Values of $K_{app}(\text{min}^{-1})$ and R^2 for MB degradation using ZnO and ZnO/Mullitecomposites	59
Table 4.5:	Performance of ZnO/Mullite for inactivation of bacteria in Zaria raw water in the dark and under illumination for 90 min	68
Table 4.6:	Rate constant and R^2 values for bacterial inactivation	70

LIST OF FIGURES

Figure 2.1:	Schematic of semiconductor excitation by band gap illumination leading to the creation of “electrons” in the conduction band and “holes” in the valance band.	9
Figure 2.2:	Mechanism of photocatalytic inactivation of microbes	30
Figure 2.3:	Inactivation of a bacterial cell	31
Figure 3.1.	Process Flow Diagram of the Experimental Procedure.	38
Figure 4.1:	XRD pattern of the synthesized ZnO	50
Figure 4.2:	XRD pattern of the synthesized Mullite	51
Figure 4.3:	Photocatalytic degradation of MB using ZnO and varying proportion of ZnO/Mullite composites under visible irradiation	57
Figure 4.4:	Pseudo first order kinetic plot for the solar photocatalytic degradation of methylene blue using the synthesized ZnO/Mullite composites	58
Figure 4.5:	<i>E.coli</i> inactivation in the dark and under visible light irradiation using 0.5g/L of the photocatalyst. a: ZnO, b: 10% ZnO/Mullite, c:20% ZnO/Mullite, d: 30% ZnO/Mullite, e: 40%ZnO/Mullite, f: 50%ZnO/Mullite	61
Figure 4.6:	<i>E.coli</i> inactivation in the dark and under visible light irradiation using 1g/L of the photocatalyst. a: ZnO, b: 10% ZnO/Mullite, c:20% ZnO/Mullite, d: 30% ZnO/Mullite, e: 40%ZnO/Mullite, f: 50%ZnO/Mullite	63
Figure 4.7:	<i>E.coli</i> inactivation in the dark and under visible light irradiation using 2g/L of the photocatalyst. a: ZnO, b: 10% ZnO/Mullite, c:20% ZnO/Mullite, d: 30% ZnO/Mullite, e: 40%ZnO/Mullite, f: 50%ZnO/Mullite	65
Figure 4.8:	<i>Salmonella</i> inactivation using selected concentration of the photocatalyst. a: 0.5g- 10%ZnO/Mullite, b: 1.0g-10%ZnO/Mullite, c: 0.5g-30% ZnO/Mullite, d: 1.0g-30%ZnO/Mullite.	66
Figure 4.9:	Control experiment using 1.0g of the support. a: <i>Ecoli</i> inactivation, b: <i>Salmonella</i> inactivation	67
Figure 4.10:	Percentage COD removal using synthesize support	69

Figure 4.11: <i>E coli</i> inactivation spectra of ZnO/mullite samples	71
Figure: 4.12 Disinfection rate constant calculation spectra of ZnO/mullite samples	71

LIST OF PLATE

Plate 1:	Scanning electron micrographs of the beneficiated kaolinite, mullite, ZnO and 20-ZnO/mullite at low magnification and high magnification.	52
----------	---	----

LIST OF APPENDICES

Appendix A: Synthesis of ZnO/Mullite Photocatalyst Calculations	84
Appendix B: Crystalline Size Determination from XRD Data	86
Appendix C: Surface Area Determination Using Sear's Method	88
Appendix D: Determination of pH at Point of Zero Charge Using Drift Method	89
Appendix E: Preliminary Photocatalytic Activity of the Synthesized ZnO And ZnO/Mullite Photocatalysts	93
Appendix F: Photocatalytic Inactivation of <i>E.Coli</i> and <i>S.enterica</i> Using the Synthesized Zno/Mullite Photocatalysts	96
Appendix G: COD Determination of Zaria Dam Raw Water Solution Under Photocatalysis.	101

LIST OF ABBREVIATIONS

AOP	Advanced Oxidation Process
BET	Brunaur – Emmett – Teller
CB	Conduction Band
COD	Chemical Oxygen Demand
<i>E coli</i>	<i>Escherichia coli</i>
hr	Hour
ISO	International Standard of Organization
JCPDS	Joint Committee on Powder Diffraction Standard
K_{app}	Apparent Rate Constant
L – H	Langmuir – Hinshelwood
MB	Methylene blue
min	Minute
NGRL	National Geological Research Laboratory
nm	Nanometer
pH _{PZC}	pH at Point of Zero Charge
SC	Semiconductor
SEM	Scanning Electron Microscopy
SiO ₂	Silica
UV	Ultraviolet
VB	Valence Band
W	Watt
XRD	X-Ray Diffraction
ZnO	Zinc oxide
θ	Diffraction angle (°)

CHAPTER ONE

INTRODUCTION

1.1 Preamble

Nearly 20% of the world's population lacks clean drinking water (Shannon *et al.*, 2008). With a rapidly increasing world population, this problem is further exacerbated. Many groundwater and surface water sources are contaminated, thus necessitating safe and reliable disinfection techniques (Kemper *et al.*, 2010).

Conventionally, water is disinfected by chlorination, which uses free chlorine as a strong oxidant. The biggest drawback to this method is the possible production of carcinogenic disinfection by-products (DBPs) such as trihalomethanes and haloacetic acids (Gopal *et al.*, 2007). Ozone is an alternative strong oxidant for disinfection of water. However, ozonation may also produce toxic DBPs during the disinfection process (Krasner *et al.*, 2006). Therefore, safe and sustainable alternative water disinfection methods are required.

Photocatalytic disinfection is considered a promising alternative due to several advantages; firstly, photocatalytic disinfection does not produce any toxic or carcinogenic disinfection by-product(DBPs). Secondly, photocatalytic materials used for disinfection can be recycled while the conventional chemical methods consume chemical disinfectants. Oxidants generated by such photocatalytic materials are strong enough to inactivate pathogenic microorganisms in water (Zhang *et al.*, 2010).

The role of zinc oxide (ZnO) in photo-induced oxygen uptake of the aqueous solutions is well reported (Yeber *et al.*, 1999). ZnO has been applied in different advanced oxidation systems for the degradation of a pulp mill ECF bleaching effluent (Yeber *et al.*, 1999). Furthermore, ZnO has been used to eliminate hazardous organic compounds, such as phenol,

from wastewaters (Fortuny *et al.*, 1999). The photodegradation of 2,3,4- halosubstituted benzyl alcohols (HBAs) with semi conductive oxides (TiO₂, ZnO) has been well studied (Wissiak *et al.*, 2000). In addition to being applied as a photocatalyst, ZnO has also been used to mimic the functions of chloroplasts in the near UV according to the electron theory of catalysis of photosynthesis (I-ji *et al.*, 1976). It has been shown that the semiconducting ZnO exhibits more rapid reactive dye degradation kinetics than anatase TiO₂(Gouvea *et al.*, 2000). It was found that *E.coli* toxicity of lignin and Kraft E1 effluent was completely removed by Ag-doped ZnO photocatalyst (Gouvea *et al.*, 2000).

Kaolin as a raw material has been commonly used in ceramic industries. After sintering kaolin at high temperatures, the main product phase is mullite (Schneider *et al.*, 1994). Because of its excellent physical properties, such as low dielectric constant, low thermal expansion, high melting point, high resistance to creep, high temperature mechanical stability, and high thermal shock and chemical corrosion resistance, mullite is an important constituent of refractories, white wares and structural clay products, and they are also widely used as electric resistor and thermal insulator (Aksel, 2003). Previous researchers (Chen *et al.*, 2000) have used many approaches to prepare mullite by solid-state reaction, coating and using sol-gel technique. In addition to those approaches, to prepare mullite using kaolin as starting material is also an important one for its economic potential.

In this study, ZnO powders was synthesized and anchored on mullite and applied as photocatalysts for photocatalytic disinfection of microorganism in water, *E.coli* and *S.enterica*. The effects of ZnO loading on the support and the rate constant were also examined.

1.2 Problem Statement

- i. In developing countries four-fifth of all illnesses are caused by water-borne diseases with diarrhea being the leading cause of childhood death. (W.H.O, 2012)
- ii Conventional methods of water disinfection such as chlorination produce a lot of disinfection by products (DBPs) which are harmful and the processes are often expensive.(Belapurkar *et al.*, 2006)
- iii Most conventional semiconductor photocatalysts such as TiO₂ and ZnO are expensive, difficult to separate after disinfection and are prone to photo-corrosion(Seven *et al.*, 2004).

1.3 Aim and Objectives

The aim of this research work is to prepare, characterize and apply ZnO/mullite composite photocatalyst for inactivation of *E.coli* and *S.enterica* of water.

The specific objectives are:

- i to prepare the ZnO/mullite composite by impregnation method.
- ii to characterize the composite using XRD, XRF,SEM, pH_{PZC} and specific surface area analyses.
- iii to evaluate the photocatalyst activity using methylene blue as contaminant
- iv to apply the synthesized photocatalyst for inactivation of *E.coli* and *S.enterica* in water under visible light illumination.

- v to study the effect of photocatalyst dosage and irradiation time on the efficiency of the inactivation process.
- vi to apply the synthesized photocatalyst to disinfect and detoxify raw water from Zaria dam using the best photocatalyst.

1.4 Justification

- i The amount of energy utilized in photocatalytic technology is provided by sunlight which is a cheap renewable energy source.
- ii The raw material and the technology needed for the synthesis of ZnO/mullite support are readily available and affordable.
- iii ZnO and mullite are environmentally friendly

1.5 Scope and Limitation

This work involves:

- i to synthesize and characterize the ZnO/mullite from zinc carbonate and Kankara kaolinite clay respectively.
- ii to investigate of the antimicrobial effects in the dark and under visible light irradiation of ZnO/Mullite on *E.coli* and *S.enterica* obtained from the Veterinary Public Health and Preventive Medicine, A.B.U Zaria.
- iii to apply the synthesized photocatalyst in the dark and under visible light irradiation to disinfect and detoxify raw water from Zaria dam

CHAPTER TWO

LITERATURE REVIEW

2.1 Photocatalysis

Photocatalysis can be defined as the acceleration of a photoreaction by the presence of a catalyst (Suresh, *et al.*, 2012).

In 1972, Fujishima and Honda discovered the photocatalytic splitting of water on TiO₂ electrodes.

Since then, research efforts in understanding the fundamental processes and in enhancing the photocatalytic efficiency of TiO₂ and other semiconductors have come from extensive research performed by chemists, physicists, and chemical engineers. Such studies are often related to energy renewal and energy storage (Bard, 1982). In recent years, applications to environmental cleanup have been one of the most active areas in heterogeneous photocatalysis. This is inspired by the potential application of TiO₂-based photocatalysts for the total destruction of organic compounds in polluted air and wastewater (Pelizzetti and Schiavello, 1988).

2.2 Types of Photocatalysis

2.2.1 Homogeneous photocatalysis

In homogeneous photocatalysis, the reactants and the photocatalysts are in the same phase. The most commonly used homogeneous photocatalysts are the ozone, the transition metal salts and the photo-Fenton systems. The mechanism of the hydroxyl radical production by the ozone is as follows,

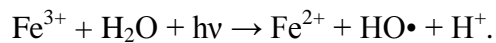


The Fenton reaction is a homogeneous photocatalytic process which does not involve light illumination. Conversely, in the Photo-Fenton system, an iron catalyst is used in the presence of hydrogen peroxide under visible light irradiation (approximately 450-600nm).

Photo-Fenton system produces hydroxyl radicals by the following mechanism



In photo-Fenton type processes, additional sources of OH radicals should be considered: through photolysis of H_2O_2 , and reduction of Fe^{3+} ions under UV light:



(2.10)

The efficiency of Fenton type processes is influenced by several operating parameters like concentration of hydrogen peroxide, pH and intensity of UV. The main advantage of this process is the ability of using sunlight with wavelength up to 450 nm, thus avoiding the high costs of UV lamps and electrical energy (Suresh, *et al.*, 2012). The disadvantages of the fenton type process are the low pH values which are required, since iron precipitates at higher pH values for the iron needs to be removed after treatment.

2.2.2 Heterogeneous photocatalysis

In heterogeneous photocatalysis two or more phases are used in the photocatalytic reaction. A light source with semiconductor material is used to initiate the photoreaction. The catalysts can carry out substrate oxidations and reductions simultaneously. UV light of long wavelengths can be used, possibly even sunlight. Most common heterogeneous photocatalysts are semiconductors, which have unique characteristics. Unlike the metals which have a continuum of electronic states, semiconductors possess a void energy region where no energy levels are available to promote recombination of an electron and hole produced by photoactivation in the solid (Jina Choi, 2010). The void region, which extends from the bottom of the filled valence band to the top of the vacant conduction band, is called the band gap. When light falls on these semiconductors, the electron present in the valence band jumps to the conduction band, a result of which is the generation of a positive hole. The recombination of the electron and the hole must be prevented as much as possible if a photocatalyzed reaction is to be favoured (Pelaez, *et al.*, 2012). The ultimate goal of the process is to have a reaction between the activated electrons with an oxidant to produce a reduced product, and also a reaction between the generated holes with a reductant to produce an oxidized product. Due to the generation of positive holes and electrons, oxidation-reduction reactions take place at the surface of semiconductors. In the oxidative reaction, the positive holes react with the moisture present on the surface and produce a hydroxyl radical.

Oxidative reactions due to photocatalytic effect are represented in Equation 2.11– 2.17.



Here MO stands for metal oxide



The reductive reaction due to photocatalytic effect is represented below:



Ultimately, the hydroxyl radicals are generated in both the reactions. These hydroxyl radicals are very oxidative in nature and non-selective with redox potential of $E_0 = +3.06$ V.

2.3 Mechanism and Fundamentals of Photocatalytic Reactions

Heterogeneous photocatalysis using UV/TiO₂ is one of the most common photocatalytic process and is based on adsorption of photons with energy higher than 3.2 eV (wavelengths lower than ~390 nm) resulting in initiating excitation related to charge separation event (gap band) . Generation of excited high-energy states of electron and hole pairs occurs when wide band gap semiconductors are irradiated higher than their band gap energy. It results in the promotion of an electron in the conductive band (e_{CB}^-) and formation of a positive hole in the valence band (h_{VB}^+). The h_{VB}^+ and e_{CB}^- are powerful oxidizing and reducing agents, respectively. The h_{VB}^+ reacts with organic compounds resulting in their oxidation producing CO₂ and H₂O as end products (see Figure 2.1). The h_{VB}^+ can also oxidize organic compounds by reacting with water to generate $\bullet OH$. Hydroxyl radical ($\bullet OH$) produced has

the second highest oxidation potential (2.80 V), which is only slightly lower than the strongest oxidant – fluorine. Due to its electrophilic nature (electron preferring), the $\bullet\text{OH}$ can non-selectively oxidize almost all electron rich organic molecules, eventually converting them to CO_2 and H_2O (Is, 2012).

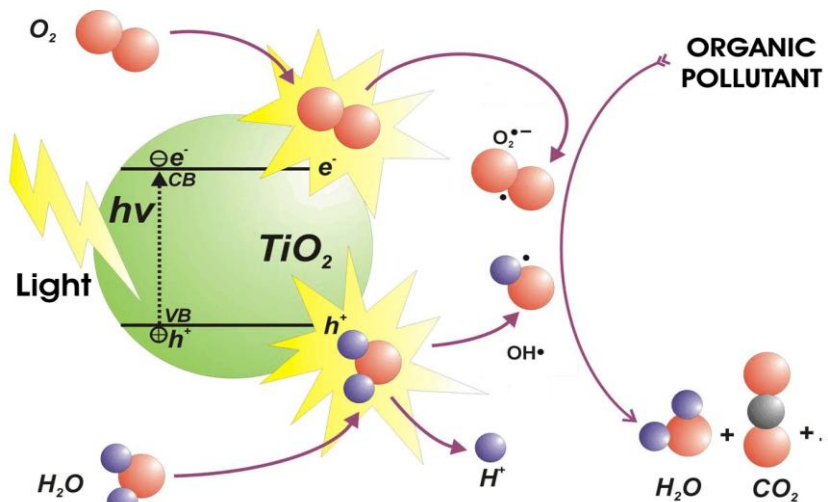


Figure 2.1: Schematic of semiconductor excitation by band gap illumination leading to the creation of “electrons” in the conduction band and “holes” in the valance band.(Fujishima, 2008)

2.4 Types of Photocatalysts and their Characteristics

A number of solids can be referred to as photocatalysts and as mentioned earlier, metal oxide semiconductors are considered to be the most suitable photocatalysts due to their photocorrosion resistance and wide band gap energies (Fox and Dulay 1993). Table 2.1 provides the band gap energies at corresponding wavelength for well-known semiconductors. TiO_2 stands out as the most effective photocatalyst and has been extensively used in water and wastewater treatment studies because it is cost effective, thermally stable, non-toxic, chemically and biologically inert and is capable of promoting oxidation of organic compounds (Mandelbaum *et al.*, 1999). The photocatalytic activity of TiO_2 is dependent on surface and structural properties which include crystal composition, surface area, particle size

distribution, porosity and band gap energy (Ahmed *et al.*, 2011). TiO₂ is also known as titania, titanic oxide, titanium white, titanic anhydride, or titanic acid anhydride.

There are several materials known for their photocatalytic potentials of which most of them are metal oxides. However, the use of titanium dioxide in photocatalysis by Honda and Fujishima in 1978, has made it the most popular photocatalytic material due to its abundance; low cost, chemical stability, biocompatibility and high efficiency under UV light (Murat, 2012). Another semiconductor that share similar properties with titanium dioxide is zinc oxide. Zinc oxide has been getting increasing attention as a photocatalytic material due to its similar electronic structure and catalytic efficiency with TiO₂. While zinc oxide can be a more efficient photocatalyst in near UV excitations compared to titanium dioxide, it has the problem of photo-corroding itself, limiting its wide use (van de Krol, Liang *et al.*, 2008).

Table 2.1. Band gap energies of various semiconductors at relevant wavelengths

Semiconductor	Band gas energy (eV)	Wavelength
TiO ₂ (rutile)	3.0	413
TiO ₂ (anatase)	3.2	388
ZnO	3.2	388
ZnS	3.6	335
CdS	2.4	516
Fe ₂ O ₃	2.3	539

(Source: Fujishima, 2008)

2.5 Radiation Sources for Photocatalysis

Both artificial visible light UV lamps and sunlight can be used as the radiation source for photocatalytic process. Artificial UV lamps containing mercury are the most commonly used source of UV irradiation. These can be divided into low pressure mercury lamp, medium

pressure mercury lamp and high pressure mercury lamp. Sunlight has also been used in the photocatalytic process as nearly 4-5% of the sunlight that reaches the earth's surface is in the 300-400 nm near UV light range. Furthermore solar energy has limitations due to the graphical variations when compared with the artificial UV lamps. However ongoing interests and developments in harnessing solar energy are expected to increase its use in photocatalytic degradation applications (Dong *et al.*, 2015).

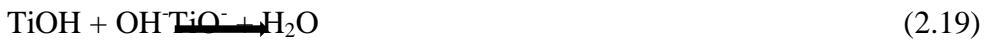
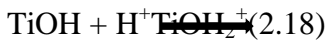
2.6 Factors Affecting the Degradation Performance

2.6.1 Catalyst loading

The amount of TiO₂ in a photocatalytic system plays a significant roll the overall photocatalytic reaction rate. The concentration of the TiO₂ particles affects the overall photocatalytic reaction rate in a true heterogeneous catalytic regime (Gaya and Abdullah, 2008). However, when the amount of TiO₂ is above certain level (saturation stage), the light photon adsorption co-efficient decreases radially and the excess photocatalyst can create a light screening effect that leads to the reduction in the surface area exposed to irradiation and thus reduces the photocatalytic efficiency of the process (Chong *et al.*, 2010). A number of studies have reported the effect of TiO₂ loadings on the treatment efficiency of the photocatalytic reactor (Chong *et al.*, 2009). Although a direct comparison between these studies is difficult due to the differences in the working geometry, radiation fluxes and wavelengths used. It was evident that the optimum dosages of photocatalyst loading were dependent on the dimension of the reactor. The importance of the determination of the reactor diameter has been emphasized to achieve effective photon absorption (Malatos *et al.*, 2009). The optimum dosage of TiO₂ used by various authors either alone or in combination with other catalysts is given in Table 2.2

2.6.2 pH of the solution

The pH is the measure of the degree of alkalinity and acidity of a solution. The effect of pH on the photocatalytic reaction has been extensively studied (Wang and Ku, 2007) due to the fact that photocatalytic water treatment is highly dependent on the pH as it affects the charge on the catalyst particles, size of aggregates and the position of conduction and valence bands (Chong *et al.*, 2010). Furthermore, the surface of the TiO₂ can be protonated or deprotonated under acidic or alkaline conditions (Gaya and Abdullah, 2008), respectively according to the reaction in Equation 2.18-2.19.



The point of zero charge for TiO₂(P25 Degussa), the most commonly used form of TiO₂ is 6.9 (Kosmulski 2006). Therefore the surface of the TiO₂ is positively charged under acidic conditions and negatively charged under alkaline conditions. The maximum oxidizing capacity of the titania is at lower pH however the reaction rate is known to decrease at low pH due to excess H⁺ (Sun *et al.*, 2006). The selection of pH is thus needed to be appropriate in order to achieve maximum degradation efficiency

Table 2.2. Optimum dosage of photocatalyst for degradation of organic compounds (dyes)

Target compound	Photocatalyst	Optimum dosage (g/L)	References
Erioglaucine	TiO ₂	0.3	Daneshvar <i>et al</i> , 2006
Tebuthionon	TiO ₂	5	Muneer <i>et al</i> , 2005
Propham	TiO ₂	5	Muneer <i>et al</i> , 2005
Triclopyr	TiO ₂	2	Qamar <i>et al</i> , 2006
Phorate	TiO ₂	0.5	Burns <i>et al</i> , 1999
Turbophos	TiO ₂	0.5	Tariq <i>et al</i> , 2005
Trichlorfon	TiO ₂	8	Tariq <i>et al</i> , 2008
Methamodiphos	Re- TiO ₂	1	Chong <i>et al</i> , 2010
Methylene blue	La-Y/TiO ₂	4	Saquib and Muneer 2003
Carbendazim	TiO ₂	0.07	Bahnemann, 2004
Direct red 23	Ag-TiO ₂	3	Bhatkhnade <i>et al</i> , 2004
Phenol	Pt- TiO ₂	1	Abdullah <i>et al</i> , 1990
Carbofuran	TiO ₂	0.1	Lin and Lin 2007
Beta-cypermethrin	RuO ₂ -TiO ₂	5	Parent <i>et al</i> , 1996
Aniline	Pt-TiO ₂	2.5	Crittenden <i>et al</i> , 1996
Benzylamine	Pt-TiO ₂	2.5	Leng <i>et al</i> , 2000
Glyphosate	TiO ₂	6	Habibi <i>et al</i> , 2005
Picloram	TiO ₂	2	Leng <i>et al</i> , 2000
Floumeturon	TiO ₂	3	Ozkan <i>et al</i> ,
2004k6			
Imazapyr	TiO ₂	2.5	Riga <i>et al</i> , 2007

2.6.3 Size and structure of the photocatalyst

Surface morphology such as particle size and agglomerate size, is an important factor to be considered in photocatalytic degradation process because there is a direct relationship between organic compounds and surface coverage of the photocatalyst (Guillard *et al.*, 2003). The number of photon striking the photocatalyst controls the rate of reaction which signifies that the reaction takes place only in the absorbed phase of the photocatalyst (Kogo *et al.*, 1980). A number of different forms of TiO₂ have been synthesized to achieve the desired characteristics of the photocatalyst (Gao and Liu, 2005). Some of the examples include UV100, PC500 and TTP. For the degradation of various organic compound such as pesticides and dyes, the efficacy of these commercial TiO₂ photocatalysts has generally been reported in the order of Degussa P25 > UV100 > PC500 > TTP (Degussa P25, Hombikat UV100, Millenium PC500, Travancore titanium product) (Tariq *et al.*, 2008).

2.6.4 Reaction temperature

An increase in reaction temperature generally results in increased photocatalytic activity, however reaction temperature greater than 80°C promotes the recombination of charge carriers and disfavor the adsorption of organic compounds on the titania surface (Gaya and Abdullah, 2008). A reaction temperature below 80°C favours the adsorption whereas further reduction of reaction temperature to 0°C results in an increase in the apparent activation energy. Therefore temperature range between 20-80°C has been regarded as the desired temperature for effective photomineralization of organic content (Chong *et al.*, 2010).

2.6.5 Concentration and nature of pollutants

The rate of photocatalytic degradation of certain pollutant depends on its nature, concentration and other existing compounds in water matrix. A number of studies have reported the dependency of the TiO_2 reaction rate on the concentration of contaminants in water (Chong *et al*, 2009). High concentration of pollutants in water saturates the TiO_2 surface and hence reduces the photonic efficiency and deactivation of the photocatalyst (Saquib and Muneer, 2003). In addition to the concentration of pollutants, the chemical structure of the target compound also influences the degradation performance of the photocatalytic reactor. For example, 4-chlorophenol requires prolonged irradiation time due to its transformation to intermediates compared with oxalic acid that transforms directly to carbon dioxide and water, i.e., complete mineralization (Bahnemann, 2004). Furthermore, if the nature of the target water contaminants is such that they adhere effectively to the photocatalyst surface the process would be more effective in removing such compounds from the solution. Therefore the photocatalytic degradation of aromatics is highly dependent on the substituent group (Gaya and Abdullah, 2008). The organic substrates with electron withdrawing nature (benzoic acid, nitrobenzene) strongly adhere to the photocatalyst and therefore are more susceptible to direct oxidation compared with the electron donating groups (Bhatkhnade *et al*, 2004).

2.6.6 Surface area

The photocatalytic activity of a semiconductor photocatalyst involves adsorption of the compound (to be oxidized) and trapping of holes and electrons on the catalyst surface. Number of trap centers is important and strongly influences the recombination rate. It is indeed, the competition between charge-carrier recombination and trapping that determines

the overall quantum efficiency of a photocatalyst. The surface area of a photocatalysts determines the number of adsorption sites.

2.6.7 Recombination

Recombination of photogenerated charge carriers is the major limitation in semiconductor photocatalysis as it reduces the overall quantum efficiency (Nishimoto, *et al.*, 1983). When recombination occurs, the excited electron reverts to the valence band without reacting with adsorbed species non-radiatively or radiatively, dissipating the energy as light or heat. Recombination may occur either on the surface or in the bulk and is in general facilitated by impurities, defects, or all factors which introduce bulk or surface imperfections into the crystal. Serpone *et al.* (2003) found that trapping excited electrons as Ti^{3+} species for example, occurred on a time scale of ~ 30 ps and that about 90 % or more of the photogenerated electrons recombine within 10 ns (Nakabayashi, *et al.*, 1983). Doping with ions, heterojunction coupling and nanosized crystals (Ohtani, 2011) have all been reported to promote separation of the electron-hole pair, reducing recombination and therefore improve the photocatalytic activity. For example, the TiO_2 crystallites of Evonik (Degussa) P25 contain a combination of anatase ($\sim 80\%$) and rutile ($\sim 20\%$). The conduction band potential of rutile is more positive than that of anatase which means that the rutile phase may act as an electron sink for photogenerated electrons from the conduction band of the anatase phase (Ibid). Many researchers attribute the high photocatalytic activity of this preparation to the intimate contact between two phases, enhancing separation of photogenerated electrons and holes, and resulting in reduced recombination.

2.7 Methods of Improving the Activity of Photocatalyst

2.7.1 Sensitization

Dye photosensitization has been reported by different groups to be one of the most effective ways to extend the photoresponse of photocatalysts into the visible region (Ohtani, 2011). Indeed these types of reactions are exploited in the well-known dye sensitized solar cells (O'Regan and Gratzel, 1991). The mechanism of the dye sensitized photo-degradation of pollutants is based on the absorption of visible light for exciting an electron from the highest occupied molecular orbital (HOMO) to the lowest unoccupied molecular orbital (LUMO) of a dye. The excited dye molecule subsequently transfers electrons into the conduction band of the photocatalysts, while the dye itself is converted to its cationic radical (Jina, 2010). The photocatalysts act only as a mediator for transferring electrons from the sensitizer to the substrate on the photocatalysts surface as electron acceptors, and the valence band of the photocatalysts remains unaffected. In this process, the LUMO of the dye molecules should be more negative than the conduction band of the photocatalysts. The injected electrons hop over quickly to the surface of titania where they are scavenged by molecular oxygen to form superoxide radical $O_2^{\bullet-}$ and hydrogen peroxide radical $\cdot OOH$. These reactive species can also disproportionate to give hydroxyl radical (Chen and Mao, 2007). In addition to the mentioned species, singlet oxygen may also be formed under certain experimental conditions. Oxygen has two singlet excited states above the triplet ground ones. Such relatively long live oxygen species may be produced by quenching of the excited state of the

photosensitizer by oxygen. The subsequent radical chain reactions can lead to the degradation of the dye (Ohtani, 2011).

Knowledge of interfacial electron transfer between semiconductor and molecular adsorbates is of fundamental interest and essential for applications of these materials. Ultrafast electron injection has been reported for many dye-sensitized photocatalysts systems. This injection depends on the nature of the sensitizer, the semiconductor, and their interaction. Asbury *et al.*, 2003, observed very different electron injection times from *femto* to *pico* second by changing the semiconductor under the same conditions.

2.7.2 Doping

Since the discovery of visible light-induced activity of nitrogen-containing titania particles by Asahi *et al.* (2001) "doping" has been a keyword for fabrication of visible light-sensitive photocatalysts; any photocatalysts with poor visible-light activity can be modified with metal or non-metal elements to be active under visible-light irradiation. There seems to be two reasons for the explosive growth in the number of papers on doped material. One might be a lack of methodology to prove visible light-induced photocatalysis. Another reason is an unclear definition of the term "doping". The meaning of "doping" is incorporation of atoms or ions in a crystalline lattice, i.e., modification of the bulk structure of crystallites, but not modification of surfaces (Suresh, 2012). If an adequate analytical method(s), if any, is (are) employed, average density of hetero atoms/ions can be determined, and if mapping of elements can be performed with higher sensitivity, spatial distribution may be elucidated. The effect of doping must be discussed on the basis of this structural information, though there have been few reports containing such discussion so far. In relation to this problem, recent papers have claimed that heptazine derivatives are produced on the surface of titania

particles in the procedure for nitrogen doping using urea as a nitrogen source and that they work as a photosensitizer and/or photocatalyst (Ohtani, 2011) i.e., nitrogen is not "doped" in the titania lattice but is included as a surface modifier. Even if introduced hetero atoms/ions are not "doped" in the lattice, it is useful to prepare modified photocatalysts with visible-light absorption by introducing hetero atoms/ions. One problem, however, is that newly appearing visible-light photoabsorption and photoinduced reaction rate under visible-light photoirradiation are often described in papers. The use of organic dyes for a photoinduced degradation test is inappropriate because those dyes might be adsorbed and work as visible-light photosensitizers, and it is preferable to show resemblance of absorption (diffuse reflection) and actions spectra, i.e., photocatalysis by doped (modified) photocatalysts can be proved through action spectrum analysis.

2.8 Particle Size

Particle size of a photocatalyst is often evaluated by Scherer's equation using data of powder X-ray diffraction (XRD) pattern. Scherer's equation is represented in Equation 2.20.

$$L = \frac{k\lambda}{\beta \cos\theta} \quad (2.20)$$

Where K is the shape factor of the particle (often take as $K=0.98$), λ is the X-ray wavelength, β is the half-maximum peak width and θ is the Bragg diffraction angle (Zhao, *et al.*, 2012). Another point to be noted is the correction of full width at half maximum (FWHM). Two kinds of correction are required; one is correction for broadening due to $K\alpha_2$ radiation, and the other is for broadening due to the optical path in the diffractometer. Generally speaking, the former and the latter corrections are made by assuming a radiation intensity ratio of $K\alpha_1$ and $K\alpha_2$ and by using FWHM of a standard large crystalline sample. There are at least three ways for the latter correction, but there seems to have been no discussion on the best way.

The simplest way, subtraction of FWHM of the standard, has often been employed. Both corrections appreciably affect the size of particles; a large error is expected without such corrections. Therefore, when the size of particles is demonstrated, the methods used for FWHM corrections should be described. The size of particles in the direction vertical to the corresponding lattice plane can be estimated using Scherer's equation. In comparison with the data obtained in another way, e.g., transmission or scanning electron microscopy, difference due to this may be observed. Furthermore, broadening of FWHM of XRD peaks is also induced by distortion of the crystalline lattice. In other words, Scherer's equation neglects the effect of crystal lattice distortion (Ohtani, 2011).

2.9 PHOTOCATALYTIC DEGRADATION KINETICS

Previous results of photocatalytic degradation kinetics indicated that the destruction rates of photocatalytic oxidation of various dyes over illuminated photocatalysts fitted the Langmuir–Hinshelwood (L–H) kinetics model (Cunningham *et al.*, 1994; Olivira-Campose *et al.*, 2003)

$$r = \frac{dC}{dt} = \frac{kKC}{1+KC} \quad (2.21)$$

Where r is the oxidation rate of the reactant (mg/l min), C is the concentration of the reactant (mg/l), t the illumination time, k the reaction rate constant (mg/l min), and K is the adsorption coefficient of the reactant (l/mg). When the chemical concentration C_0 is small the above equation can be simplified to an apparent first-order equation. This simplified equation (Equation 2.22) is used evaluate the apparent rate constants for the photodegradation of methylene blue.

$$\ln\left(\frac{C_0}{C}\right) = kt \quad (2.22)$$

A plot of $\ln C_0/C$ versus time represents a straight line, the slope of which upon linear regression equals the apparent first-order rate constant k . Generally, first-order kinetics is

appropriate for the entire concentration range up to a few ppm and several studies were reasonably well fitted by this kinetic model. It has been agreed that the expression for the rate of photomineralization of organic substrates such as dyes with irradiated photocatalysts follows the Langmuir–Hinshelwood (L–H) law for the four possible situations:-

- (a) The reaction takes place between two adsorbed substances.
- (b) The reaction occurs between a radical in solution and an adsorbed substrate molecule.
- (c) The reaction takes place between a radical linked to the surface and a substrate molecule in the solution.
- (d) The reaction occurs with both species being in the solution.

In all cases, the expression for the rate equation is similar to that derived from the L–H model, which has been useful in modelling the process, although it is not possible to find out whether the process takes place on the surface, in the solution or at the interface (Tanak and Reddy, 2002).

2.10 CHARACTERIZATION OF PHOTOCATALYSTS

2.10.1 X-ray diffraction (XRD) spectroscopy

X-ray diffraction (XRD) is used for examining the crystal structures of photocatalysts particles. It is a method of determining the arrangement of atoms within a crystal, in which a beam of X-rays strikes a crystal and diffracts into many specific directions using a diffractometer. It provides detailed information on the crystallographic structure and physical properties of materials and thin films (Okada *et al.*, 1986).

2.10.2 X-Ray florescence (XRF) spectroscopy

X-ray fluorescence is the emission of characteristic “secondary” (or fluorescent) X-rays from a material that has been excited by bombarding with high energy X-rays or gamma rays. The phenomenon is widely used for elemental and chemical analysis of minerals.

2.10.3 X-ray photoelectron spectroscopy

In photocatalysis, use of X-ray photoelectron spectroscopy (XPS) was not frequent before 2000 (Ohtani, 2011). The reason may be that XPS gives information on valency of elements on and near the surface of photocatalysts, but the valency of elements in the bulk of photocatalysts can be elucidated by analyzing the crystal structure by X-ray diffraction (XRD) analyses. In 2001, Asahi *et al.*, 2001 reported doping of titania with typical-elements could induce photocatalytic activity under visible-light irradiation, and the chance of using XPS has explosively increased, since analysis of valency of doped (or attached) element(s) is important to understand the structure of doped samples.

2.10.4 UV-Vis Absorption

The absorbance of any specie in solution can be determined using the Beer-Lambert’s law. This absorbance can be converted to concentration to determine the concentration of any given specie in a sample.

Beer-Lambert’s law

According to the Lambert-Beer Law, (Chun and Yizhong, 1999) the absorbance (A) of methyl orange (MO) is proportional to its concentration (c), this generally followed the following equation:

$$A = \epsilon bc. \quad (2.23)$$

Where ϵ is the molar absorption coefficient and b is the thickness of the absorption cell. In experiments, all the testing parameters are kept constant, so that ϵ and b can be considered as a constant. Therefore, the changes of the concentration (c) of MO aqueous solution can be determined by a UV-Vis spectrophotometer. As for the MO aqueous solution with low concentration, its photocatalytic decolorization is a pseudo-first-order reaction and its kinetics may be expressed as follows (Rashed and El-Amin, 2007).

$$\ln A = \ln A_0 + kt. \quad (2.24)$$

where k is the apparent rate constant and A_0 and A_t are the initial and reaction absorbance of aqueous solution, respectively. However in this dissertation, all the absorbances obtained from the UV-Vis spectrophotometer were converted to concentration from Equation 2.23.

2.10.5 Brunauer-Emmett-Teller (BET)

A Brunauer-Emmett-Teller (BET) analysis is a test to determine the surface area of photocatalysts. The surface area also depends on the crystal size of the photocatalysts which can be determined using Scherer's equation (Equation 2.20) (Okada *et al.*, 1986).

2.11 KAOLINITE

Kaolinite is a clay mineral, part of the group of industrial minerals, with the chemical composition $\text{Al}_2\text{Si}_2\text{O}_5(\text{OH})_4$. It is a layered silicate mineral, with one tetrahedral sheet linked

through oxygen atoms to one octahedral sheet of alumina octahedra. Rocks that are rich in kaolinite are known as kaolin or china clay. Kaolinite has a low shrink–swell capacity and a low cation-exchange capacity. It is a soft, earthy, usually white mineral (dioctahedral phyllosilicate clay), produced by the chemical weathering of aluminium silicate minerals like feldspar. In many parts of the world, it is colored pink-orange-red by iron oxide, giving it a distinct rust hue. Lighter concentrations yield white, yellow or light orange colors (Bergaya and Lagaly, 2013).

2.11.1 Structural transformations of Kaolinite

Kaolinite group clays undergo a series of phase transformations upon thermal treatment in air at atmospheric pressure. Below 100 °C (212 °F), exposure to dry air will slowly remove liquid water from the kaolin. The end-state for this transformation is referred to as "leather dry". Between 100 °C and about 550 °C (1,022 °F), any remaining liquid water is expelled from kaolinite. The end state for this transformation is referred to as "bone dry". Through this state, the expulsion of water is reversible: if the kaolin is exposed to liquid water, it will be reabsorbed and disintegrate into its fine particulate form. Subsequent transformations are *not* reversible, and represent permanent chemical changes (Ibarra *et al.*, 2015)

Endothermic dehydration of kaolinite begins at 550–600 °C producing disordered metakaolin, but continuous hydroxyl loss is observed up to 900 °C (1,650 °F). Although historically there was much disagreement concerning the nature of the metakaolin phase, extensive research has led to a general consensus that metakaolin is not a simple mixture of amorphous silica (SiO₂) and alumina (Al₂O₃), but rather a complex amorphous structure that

retains some longer-range order (but not strictly crystalline) due to stacking of its hexagonal layers (Bergaya and Lagaly, 2013).



Further heating to 925–950 °C converts metakaolin to an aluminium-silicon spinel which is sometimes also referred to as a gamma-alumina type structure:



Upon calcination above 1050 °C, the spinel phase nucleates and transforms to platelet mullite and highly crystalline cristobalite:



Finally, at 1400 °C the "needle" form of mullite appears, offering substantial increases in structural strength and heat resistance. This is a structural but not chemical transformation

2.12 Mullite

Mullite or porcelainite is a rare silicate mineral of post-clay genesis. It can form two stoichiometric forms $3\text{Al}_2\text{O}_3 \cdot 2\text{SiO}_2$ or $2\text{Al}_2\text{O}_3 \cdot \text{SiO}_2$. Unusually, mullite has no charge balancing cations present. As a result, there are three different Al sites: two distorted tetrahedral sites and one octahedral.

Mullite is the only stable intermediate phase in the alumina–silica system at atmospheric pressure. Although this solid solution phase is commonly found in human-made ceramics, only rarely does it occur as a natural mineral. Yet mullite is a major component of aluminosilicate ceramics and has been found in refractories and pottery dating back millennia. As the understanding of mullite matures, new uses are being found for this ancient

material in the areas of electronics and optics, as well as in high temperature structural products. Many of its high temperature properties are superior to those of most other metal oxide compounds, including alumina(Ibarra *et al.*, 2015).

The Properties of mullite are:

1. Good thermal shock and stress resistance
2. Low thermal conductivity
3. Good strength
4. Wear resistant
5. Usable to high temperatures

Application of mullite:

1. Use in protection of tubes
2. Use in furnace liner
3. Use in electrical insulators
4. Use as support material

(Source: Journal.Eur.Ceram.Soc. 35(2015) 2189-2194)

2.13 ZINC OXIDE

Zinc oxide is an inorganic compound with the formula ZnO . Zinc oxide is a white powder that is insoluble in water, and it is widely used as an additive in numerous materials and products including rubbers, plastics, ceramics, glass, cement, lubricants, paints, ointments, adhesives, sealants, pigments, foods, batteries, ferrites, fire retardants, and first-aid tapes. It occurs naturally as the mineral zincite, but most zinc oxide is produced synthetically(Betencet *al.*, 2008).

ZnO is a wide-bandgap semiconductor of the II-VI semiconductor group. The native doping of the semiconductor due to oxygen vacancies or zinc interstitials is n-type. This semiconductor has several favorable properties, including good transparency, high electron mobility, wide bandgap, and strong room-temperature luminescence. Those properties are used in emerging applications for transparent electrodes in liquid crystal displays, in energy-saving or heat-protecting windows, and in electronics as thin-film transistors and light-emitting diodes (Kumaret al., 2010).

2.14 Water Disinfection

To get water that can be used in daily life without fearing of diseases, it must be purified and disinfected before being used. Water disinfection means the removal, deactivation or killing of pathogenic microorganisms. Microorganisms are destroyed or deactivated, resulting in termination of growth and reproduction. Sterilization is a process related to disinfection. However, during the sterilization process all present microorganisms are killed, both harmful and harmless microorganisms. Disinfection can be chemical or physical. For physical disinfection of water several disinfectants can be used such as: Ultraviolet light (UV), Electronic radiation, Gamma rays and Heat. For chemical disinfection of water several disinfectants can be used such as Chlorine dioxide (ClO_2), hypochlorite (OCl^-), ozone (O_3), halogens including chlorine (Cl_2), bromine (Br_2) and iodine (I_2), metal ions such as copper (Cu^{2+}) and silver (Ag^+), potassium permanganate (KMnO_4), alcohols, soaps, detergents, quarternary ammonium salts, hydrogen peroxide, in addition to different acids and bases. Table (2.3) summarizes advantages and disadvantages of some water disinfectants (Sihem *et al.*, 2014).

2.14.1 Disinfection by oxidation processes

Advanced Oxidation Processes (AOP) are among the newer chemical techniques used for water purification. They can be divided into two types depending on the techniques used, namely: abiotic degradation (such as thermal degradation/combustion, molten salt processes, wet oxidation, chemical oxidation or acid-base hydrolysis) and photodegradation (by $\text{H}_2\text{O}_2/\text{UV}$, O_3/UV or $\text{O}_3/\text{H}_2\text{O}_2/\text{UV}$ processes, solar photolysis, processes in vacuum ultraviolet or photo-catalysis) (Crosby, 1998). Other water disinfection procedures involve formation of disinfecting by-products (DBPs). Important examples are the trihalomethanes (THMs). Such processes have limited use due to their carcinogenic and mutagenic nature (Richardson *et al*, 1996). They result from chlorination of groundwater with high total organic carbon (TOC) content. To decrease DBPs formation, it will be better to decompose organic compounds prior to chlorine addition. Solar disinfection by photo-catalysis has the advantage of destroying the bacterial population and DBPs as well.

Table 2.3 Comparison of the Main Water Disinfectants

Disinfectant	Advantages	Limitation
Chlorine	Very effective for killing most microbial pathogens	Dangerous and lethal at concentration as low 1% air by vol. Generation of toxic byproducts
Chlorindioxide	Very effective even in low concentration, does not generate chlorinated phenol and THMs	Has pungent odour. Should be stored in a dark area.
Sodium hypochlorite solution	Easier to handle. No disinfection byproducts	Very corrosive and should not be stored for more than a month
Solid calcium hypochlorite	Very stable when package allowing long time storage	Corrosive with strong odour, readily absorbs moisture to form chlorine gas.
Chloramins	Effective bactericide. Produces fewer DPBs, forming reactions are 99% complete within few minutes	A weak disinfectant much less effective against viruses or protozoa, detrimental reaction produces nitrogen trichloride
Ozonation	Requires shorter contact time and dosage than chlorine,	Ozone gas is very unstable and must be generated onsite, requires

	more effective than chlorine in destroying pathogens	complicated equipment and efficient contacting system, extremely irritating and possible toxic
Ultraviolet light	Readily available, produces no known toxic residual, requires short contact time and the equipment is easy to operate and maintain	May not inactivate <i>Giardia lamblia</i> or cryptosporidium cyst, unsuitable for water with high level of suspended solid, turbidity colour or soluble organic matter which can react or absorb the UV radiation

(Source: National drinking water clearing house, 2011)

2.15 DISINFECTION MECHANISMS

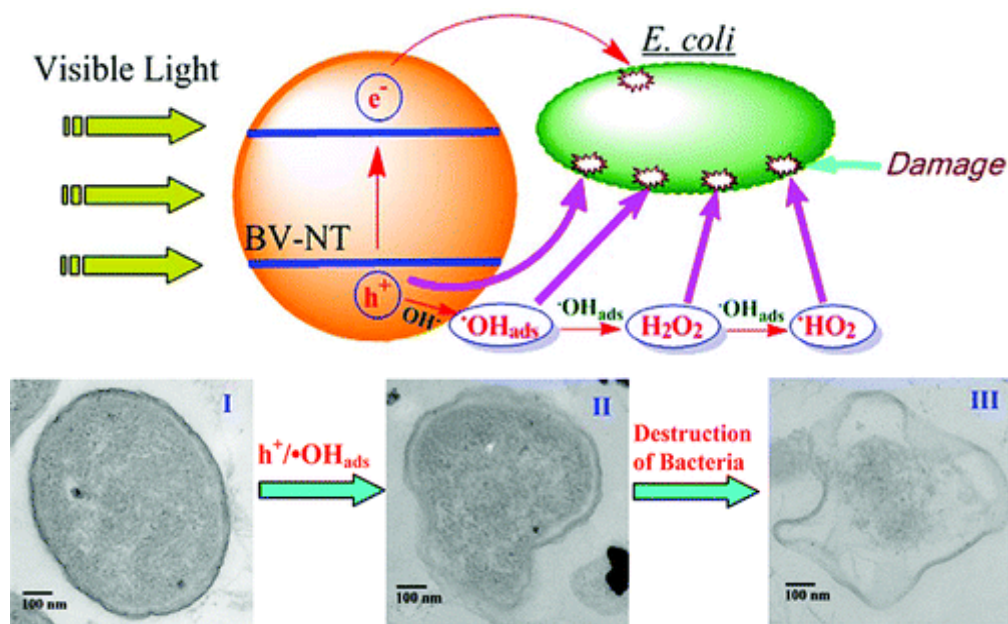


Figure 2.2: Mechanism of photocatalytic inactivation of microbes (Wang *et al.*, 2012)

Disinfection commonly takes place by: destroying cell wall of microorganisms, inhibiting proteins or nucleic acids synthesis, changing cell membrane permittivity and antagonizing enzymes action (structural change in enzymes). These disturbances in cell activity cause

microorganisms to no longer be able to multiply. This causes the microorganisms to die out. Oxidizing disinfectants also demolish organic matter in the water, causing a lack of nutrients.

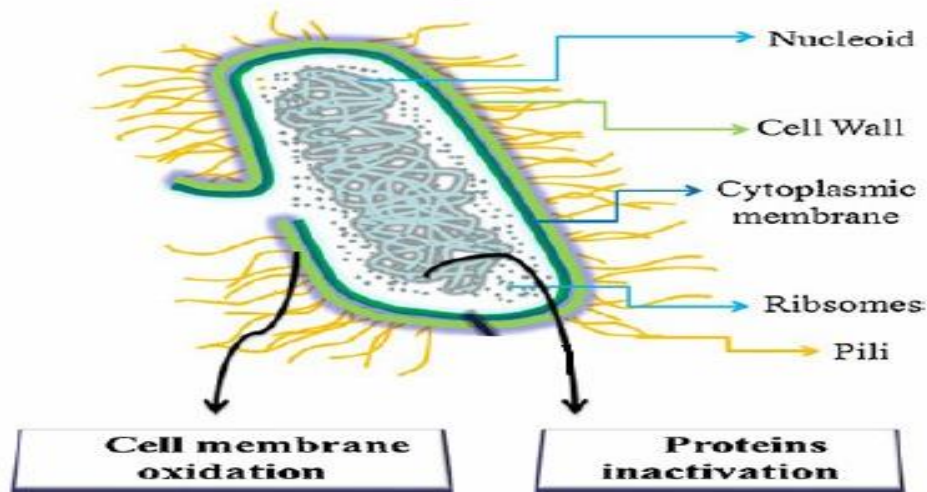


Figure 2.3: Inactivation of a bacterial cell(Pan *et al.*, 2010)

2.16 Microorganisms

Microorganisms are invisible to bare eyes and are present in soil, air, food and water (Burke, 1993). Through consumption of food and air people are exposed to microorganisms. Most microorganisms are harmless and will contribute to a number of vital processes in the human body, such as the metabolism (there is a bacterium in the human gut which help in synthesizing vitamin like biotin, vitamin k and folic acid). However, there are also microorganisms which can cause disease or which are harmful to people with low resistance to disease (example, people with low immune system). Pathogenic microorganisms in water can be distinguished from chemical contaminants. Microorganisms are living organisms and

are not dissolved in water, but they will coagulate or attach to colloids and solids in water(Wanjun *et al.*, 2012).

2.16.1 Types of pathogenic microorganisms

Pathogenic microorganisms in drinking water can be divided into three types: bacteria, viruses and parasitic protozoa. Bacteria and viruses can exist in both surface water and groundwater, whereas parasitic protozoa can be found mainly in surface water (Tortora, 2008).

2.16.2 Bacteria

Bacteria are the most abundant life-form on earth. They are single cell organisms, they can be found in different shapes; a sphere, a spiral or a rod. They occur as individual bacteria or in bacterial chains, bundles or pairs. Their length normally between 0.40 and 14×10^6 m and the width is about 0.20 to 12×10^6 m. Consequentially they can only be viewed under a microscope. They can reproduce by means of DNA replication, causing a bacterium to split into two independent cells. The replication process takes about 15 to 30 minutes in ideal circumstances. Bacteria are enclosed in cell walls that are largely composed of a carbohydrate and protein complex called *peptidoglycan* (Petit *et al.*, 2007). Bacteria generally reproduce by dividing into two equal cells (*binary fission*). Most bacteria use organic chemicals for nutrition, which can be obtained from either dead or living organisms.

Some bacteria can manufacture their own food by photosynthesis, and some can derive nutrition from inorganic substances (Tortora *et al.*, 2010).

2.16.3 *Escherichia coli* (*E. coli*)

The bacterial species *Escherichia coli* is one of the most common inhabitants of the human intestinal tract and is probably the most familiar organism in microbiology. Optimal growth of *E. coli* occurs at 37°C, and the optimum pH growing in a culture at 37°C is 6.0-7.0. It has a minimum pH level of 4.4 and a maximum level of 9.0 required for growth. It is a facultative anaerobes organism that can grow in either the presence or absence of oxygen. It is used frequently as biological indicator of disinfection efficiency in water systems. They are a large and diverse group of bacteria. Although most strains of *E.coli* are harmless, others can cause some diseases; some kinds of *E.coli* can cause diarrhea, while others cause urinary tract infections, respiratory illness and pneumonia and other illnesses (Ranjith *et al.*, 2011).

The presence of *E.coli* in recreational waters is used to indicate fecal contamination and the possible presence of other more pathogenic microorganisms such as *Salmonella*, *Shigella*, *Campylobacter*, *Giardia*, *Cryptosporidium* or *Norovirus* (Sampson *et al.*, 2006).

2.16.4 *Salmonella enterica*

Salmonella enterica are non-spore-forming, predominantly motile enterobacteria with diameters around 0.7 to 1.5×10⁶m, lengths from 2 to 5 ×10⁶m, and peritrichous flagella (flagella that are all around the cell body) (Fabrega and Vila, 2013). They are chemoorganotrophs, obtaining their energy from oxidation and reduction reactions using organic sources, and are facultative anaerobes. Many infections are due to ingestion of contaminated food. They can be divided into two groups; typhoidal and nontyphoidal *Salmonella* serovars. Nontyphoidal serovars are more common, and usually cause self-

limiting gastrointestinal disease (Fabrega and Vila, 2013). They can infect a range of animals, and are zoonotic, meaning they can be transferred between humans and other animals. Typhoidal serovars include *Salmonella* Typhi and *Salmonella* Paratyphi A, which are adapted to humans and do not occur in other animals (Fabrega and Vila, 2013).

2.17 Some Previous Related Works

Wang *et al.*(2012) carried out a study on visible-light-driven photocatalytic inactivation of *E.coli* k-12 by bismuth vanadate nanotubes bactericidal performance and mechanism. The visible light driven (VLD) photocatalytic bacterial inactivation by BV-NT did not allow any bacterial regrowth. The photogenerated h^+ and reactive oxidative species were the major reactive species for bacterial inactivation. Is (2012) studied the photocatalytic antibacterial activity of ZnO / hectorite and ZnO / montmorillonite. These materials were evaluated as photocatalyst and used to inactivate *Eschericia coli* and *Staphylococcus aureus* under UV illumination. Result of the research showed the significant activity of the photocatalysts and the higher activity of Zn/HEC compared to Zn/MMT was obtained. The possible reason for increased photoactivity was the higher specific surface area of the material(Zn/HEC).

Vineetha *et al.*(2013) investigated the photocatalytic colour and COD removal in the distillery effluent by solar radiation. They concluded that the photocatalytic degradation process using solar light as an irradiation source with a semiconductor (TiO_2/H_2O_2) showed potential reduction in the COD and colour removal by 68% of the distillery effluent treatment.

Sihem *et al.*(2014) carried out solar photocatalysis, a green technology for *E.coli* contaminated water disinfection and also studied the effect of concentration and different

types of suspended photocatalyst. The solar photo-inactivation yielded complete inactivation results, which varied with the solar light intensity. The adding of any kind of photo-catalyst to the water accelerated the bactericidal action of solar irradiation and led to complete disinfection (until detection limit). The photocatalytic disinfection efficiency was not enhanced by the increase of catalyst concentration above 0.5 g/L.

Several semiconductors photocatalyst have being used by several researchers for water disinfection and detoxification. Unfortunately each semiconductor used has its shortcoming. Some these includes; being active under UV irradiation and UV accounts for only about 5% of the solar spectrum. Other semiconductor photocatalysts such as TiO_2 and ZnO are expensive, difficult to separate after disinfection and are prone to photo-corrosion. The motivation of this research is geared towards addressing the research gap faced by other researchers in the field of photocatalysis.

CHAPTER THREE

MATERIALS AND METHODS

Enumerated are the materials and equipment used in carrying out this research work. Most of the chemicals were procured from Haddis Chemicals Nigeria Limited, Zaria.

3.1 Materials

1. Zinc carbonate. (Analytical grade, BDH Chemical England)
2. Sodium chloride. (Analytical grade, BDH Chemical England)
3. Sodium Hydroxide. (Analytical grade, BDH Chemical England)
4. Hydrochloric acid. (Analytical grade, BDH Chemical England)
5. Methylene Blue. (Guarantee reagent) grade.
6. Conical Flask (500 ml, 2000 ml) Pyrex.
7. Beaker (500 ml) Pyrex.
8. Measuring Cylinder (1000 ml, 500ml).
9. Spatula.
10. Filter Paper (grade1, 110 mm).
11. Disposable petri dishes (150×25 mm).
12. Funnel (pyrex, 20 mm).
13. Water Bath(gallenkamp, England).
14. Glass Rod Stirrer.
15. Crucibles.
16. Thermometer (Analogue).
17. Retort stand.
18. Eosin Methylene Blue (EMB)

19. Nutrient Broth Powder (Sigma-Aldrich)
20. Lactose Powder (Sigma-Aldrich)
21. MacConkey Agar (Sigma-Aldrich)
22. Kankara Kaolin (Katsina, Nigeria)

Table 3.1. List of equipment used and their specifications

S/No	Name	Model	Manufacturer
1.	Flask shaker	SF1	Gallenkamp, England
2.	Digital Weighing Balance	AB 204 (0 – 180g)	Mettler Toledo, Switzerland
3.	Halogen lamp	500 W	
4.	Oven	TMOV – 420 (0–260 °C).	Gallenkamp, England
5.	Furnace	LH 120/14 (30–3000 °C)	Nebertherm GmbH, Germany
6.	Autoclave	HIPL-001	Hexatec, India
7.	X – Ray Diffractometer	Empyrel	PANalytical, Netherlands
8.	Scanning electron Microscope Machine	Phenom pro-X	Phenomworld, Netherland
9.	UV–Vis Spectrophotometer	UV- 2500S	Shimadzu
10.	pH, Conductivity, TDS metre	HI 9A129	Portable Hanna combo

The beneficiated kaolinite clay was mixed with the zinc carbonate in various proportion by impregnation. This mixed proportions were then calcined and characterized. The characterized samples were the subjected to photocatalysis evaluations. Figure 3.1 gives the process flow diagram forthe experimental procedure.

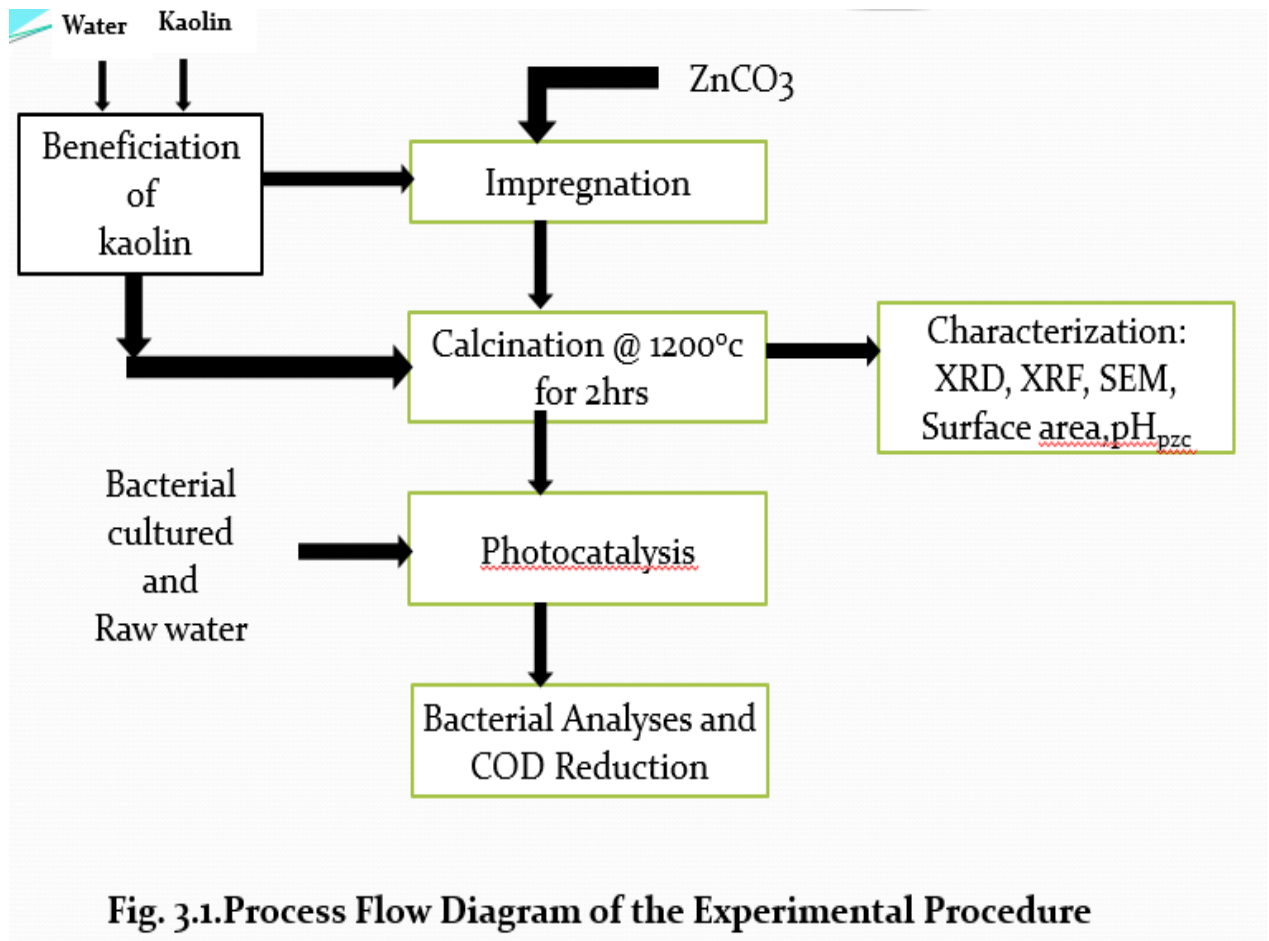


Fig. 3.1. Process Flow Diagram of the Experimental Procedure

3.2 Wet Beneficiation of Kankara Kaolin Clay

Raw kankara kaolin, procured from kankara village, in Katsina state was crushed using a mortar and pestle. It was then soaked in tap water (inside a plastic bucket) and properly plunged to break up the small lumps and the colloidal suspension was allowed to stand for three (3) days. During this period it was periodically stirred and fresh water added after removing the previous day's water by decantation. This was to remove the soluble impurities in the clay. The kaolin suspension was thereafter sieved twice using a 50 micron sieve in order to get rid of the intermediate coarse particles on the third day.

A sample from the clay fraction was taken at this stage before series of decantation rounds on the slurry ($\leq 50\mu\text{m}$ clay fraction) to ensure near complete removal of free silica, which are close to kaolin in particle size distribution but seemingly heavier in mass (Othmer, 1997). The kaolin fraction obtained at this stage is referred to as fully beneficiated sample. Prior to analyses all the samples were dried at 120°C over night to ease handling and obtain zero moisture content. Subsequently, the fully beneficiated sample was characterized using X-ray spectrometry.

3.3 Preparation of ZnO/ Mullite Photocatalyst

Pure basic zinc carbonate (ZnCO_3) manufactured by SIGMA-ALDRICH, containing from 58-61 wt. % Zn, was used alongside with beneficiated kaolinite clay obtained from Kankara. The basis for the ZnO/Mullite support is 50g per sample. Stoichiometric calculation was carried out to determine the required amount of zinc carbonate to be mixed with the kaolinite (Appendix A). Five different samples with ZnO content ranging from 10% - 50% were prepared alongside with the control for the experiment. These prepared samples were calcined at 1200°C for 2 h.

Table 3.2 gives a summary for the synthesized ZnO/Mullite support.

Table 3.2: Amount of ZnCO₃ mixed with kaolinite clay for photocatalyst preparation.

% wt (ZnO/mullite)	ZnCO ₃ (g)	Kaolin (g)	Sample label
10	7.70	45	10-ZnO/Mullite
20	15.41	40	20-ZnO/Mullite
30	23.11	35	30-ZnO/Mullite
40	30.81	30	40-ZnO/Mullite
50	38.51	25	50-ZnO/Mullite

3.4 Characterization of the Synthesized ZnO/ Mullite Support

3.4.1 Determination of point of zero charge (pH_{pzc})

The point of zero charge was carried out to determine the surface charge of the ZnO and its composites. Exactly 0.1 M KCl was prepared and its initial pH was adjusted between 2.0 and 12.0 (11 different samples) by adding either NaOH or HCl. Then, 25 mL of prepared 0.1 M KCl was taken in 100 mL flasks and 50mg of sample was added to each solution. These flasks were shaken via shaker machine for 1 hour and the final pH was measured and plotted against the initial pH. The point of intersects between the final and initial pH represents the point of zero charge (pH_{PZC}) of the sample (Zhai *et al.*, 2008).

3.4.2 Specific surface area determination (Sear's method)

The surface areas of the unsupported and supported ZnO were determined using Sear's method. This analysis was done by agitating 1.5 g of the photocatalyst sample in 100 ml of diluted hydrochloric acid of a pH of 3; 30 g of sodium chloride was then added with constant stirring and the volume was made up to 150 ml with deionized water. The solution was titrated with 0.10 N NaOH and the volume needed to raise the pH from 4 to 9 was recorded. The specific surface area of synthesized photocatalyst was estimated using equation 3.1. (Sears, 1956).

$$S (\text{m}^2 \cdot \text{g}^{-1}) = 32V - 25. \quad (3.1)$$

where S and V are the specific surface area in $\text{m}^2 \cdot \text{g}^{-1}$ and volume of NaOH in cm^3 respectively

3.5 Photocatalytic Degradation of Methylene Blue

Methylene blue (MB) was used as an inorganic contaminant for the preliminary photocatalytic activity for both the supported and unsupported ZnO samples. Exactly 10mg/L of MB was prepared as stock solutions. 0.1g of unsupported ZnO and the various proportions of the supported ZnO (10%, 20%, 30%, 40% and 50%) were added unto 100ml of MB solution (0.1g/100ml), then shaken for 1h (using a flask shaker) in dark to reach adsorption-desorption equilibrium after which it was then exposed to visible illumination. The light experiment lasted for 60 min. Aliquots were taken at 10 min interval. These aliquots were filtered, and analyzed using a UV-Vis spectrophotometer. Absorbance data were taken at λ_{max} of 665nm. The percentage degradation was calculated using equation 3.2;

$$\text{Degradation (\%)} = \frac{A_0 - A_t}{A_0} \times 100\% .$$

(3.2)

Where A_0 is the maximum absorbance at time zero ($t=0$) and A_t is the maximum absorbance on the absorption spectra of the MB solutions over time ($t_{(\text{min})} = 10, 20, 30, 45, 60$).

The pseudo first- order kinetic model was used to determine photodegradation rate constant (k_{app}) of the contaminant using equation 3.3

$$\ln \frac{C_0}{C_t} = k_{\text{app}} t \quad (3.3)$$

where K_{app} is the apparent photodegradation rate constant and C_0 and C_t are the initial and final concentrations of methylene blue solution after irradiation time, t , respectively.

3.6 Preparation of Bacterial Cultures

Nutrient agar was used as growth medium for measuring the remaining concentration of bacteria after the photo-degradation process by plate counting method. The nutrient agar media was prepared by dissolving 28 g in 1 L distilled water and poured in Petri dishes after being autoclaved. The inoculum of microorganisms was prepared using 4 h cultured nutrient broth at 37°C. The broth was prepared by dissolving 13 g in 1L distilled water. Saline solution (0.9%) was prepared by dissolving 9.00 g NaCl in 1.00 L distilled water. The solutions were then used to prepare suitable dilutions for the remaining bacteria in the contaminated water samples after reaction stoppage. After dilution, the remaining bacteria were cultured on nutrient agar to achieve countable number of colonies on the plates. Prior to use in bacterial contamination and disinfection experiments, each water sample, was

prepared by pouring 50 ml of distilled water in a 100 ml beaker. Each beaker was then charged with a magnetic stirrer and tightly stoppered with aluminum foil to prevent external contamination. All solutions were autoclaved at 121°C under 1.5 atm, and all procedures was done under sterile conditions.

3.7 Bacterial Photo-Inactivation Experiments

ZnO/Mullite and naked ZnO in both micro scales were used as photocatalysts for bacteria inactivation experiments. The catalyst (0.5g, 1 g, 1.5g, 2 g) was added to 50 ml distilled water pre-contaminated with *E coli* bacteria ($\sim 2 \times 10^6$ cfu/ml) in 100 ml conical flask attached to a flask shaker. The conical flask was agitated in the dark for 90min and aliquots were taken at 30 min interval. This process was also carried out under visible light illumination at room temperature. Mullite was used in dark to know if it affects *E coli* bacteria growth. A sample was also exposed to light without addition of catalyst to examine light effect on bacteria.

In addition, *Salmonella enterica* was used in the photo inactivation process, ZnO/mullite and naked ZnO in both micro scales were used for bacteria inactivation experiments. The catalyst (0.5 g, 1 g) g was added to 50 ml distilled water pre-contaminated with *E. coli* bacteria ($\sim 2 \times 10^6$ cfu/ml) in 100 ml conical flask attached to a flask shaker. The conical flask was agitated in the dark for 90min and aliquots were taken at 30 min interval. This process was also carried out under visible light illumination at room temperature. Mullite was used in dark to know if it affects *salmonella* growth. A sample was also exposed to light without addition of catalyst to examine light effect on bacteria.

3.7.1 Measuring the residual concentration of bacteria

After 90 min (end of the selected time) 1 ml of the treated sample was withdrawn using a micropipette and diluted in a series of saline solution tubes at different dilutions, 10^{-1} , 10^{-2} and 10^{-3} . Aliquot of 100 μl was pipetted from each tube, cultured onto an appropriate media plates and incubated at 37°C for 24 h. Then the residual concentration of bacteria was calculated using plate count method, normalized to per ml water, reported, and compared with the initial concentration in the control sample that was prepared using the same concentration of bacteria in the same volume of water but without adding anything to or exposing to any type of light. The degradation percent was calculated as represented in Equation 3.4.

$$\text{Degradation (\%)} = \frac{N_0 - N_t}{N_0} \times 100\%. \quad (3.4)$$

where N_0 is the initial bacterial concentration,

N_t is the final bacterial concentration

3.8 Measurement of COD

Five millilitres (5.0 mL) of conc. H_2SO_4 was placed into refluxing flask and 20 ml of aliquot was added, then 10 ml of standard $\text{K}_2\text{Cr}_2\text{O}_7$ solution. 30 ml $\text{AgSO}_4 - \text{H}_2\text{SO}_4$ solution was added slowly with gentle swirling, then the flask was connected to the condenser. The blank mixture was prepared and allowed to reflux for 2 h, cooled at room temperature and the condenser was washed with distilled water, the cooled sample was then poured into Erlenmeyer flask and diluted to 150 ml then allowed to cool to temperature and then titrated the excess dichromate as standard using 2 to 3 drops of ferroin as the indicator to the end point. The color change will be sharp, changing from a blue-green to a reddish hue.

$$\text{COD} = \frac{(a-b) \times c \times 8000}{\text{Volume of sample used}}. \quad (\text{See appendix G})$$

3.8.1 Measurement of pH

The electrode meter was set to pH mode and immersed into the liquid sample and the pH reading was recorded.

3.8.2 Measurement of Conductivity

The electrode meter was set to conductivity mode and immersed into the liquid sample and the conductivity of the sample was then recorded.

3.8.3 Measurement of total dissolved solid (TDS)

The electrode meter was set to TDS mode and immersed into the liquid sample and the total dissolved solid of the sample was recorded.

3.9X-RAY SPECTROMETRY

3.9.1 Sample Preparation

Pulverization:

The samples were pulverized (grind to fine powder) using arget pulverizing machine (planetary micro mill pulverisette 7). The ground samples were ensured to pass 150 micro mesh sieves. This was to ensure homogeneity of the samples.

Pelletization:

5g of the pulverized sample was weighed into a beaker, 1g of binding aid (Starch soluble). The mixture was thoroughly mixed to ensure homogeneity, which was pressed under high pressure (6 “tone”) to produced pellets; labeled and package ready for the analysis.

3.9.2 Procedure of the analysis:

The pellets were carefully placed in the respective measuring positions on a sample changer of the machine. The following condition sets were made as the machine was switched on.

1. Nature of the samples to analyzed as press powder (pellet)
2. The current used as 14kv for major oxides, 20kv for the trace elements/rare earth metals.
3. Selected filters were “kapton” for major oxides, Ag/Al-thin for the trace elements/rare earth metals.

The selection of filters was guided by a given periodic table used for elemental analysis. Time of measurement for each sample was 100 seconds and the medium used was air throughout.

The machine was then celebrated by the machines gain control, after which the respective samples were measured by clicking the respective positions of the sample changer.

LOI was determined gravimetrically by heating 1g of the powdered sample in a cleaned weighed crucible at 1000°C. After which the crucible and the content was weighed to get the difference in weight before and after heating.

$$\text{LOI} = (a-b/1) \times 100\% = \text{H}_2\text{O}^+$$

where a = weight of crucible + 1g of the sample before heating

b = weight of crucible + 1g of the sample after heating.

3.10 X-Ray Diffraction

A few tenths of a gram of the samples were obtained, as pure as possible and grinded to a fine powder, typically in a fluid to minimize inducing extra strain (surface energy) that can offset peak positions, and to randomize orientation. Powder less than 10×10^6 m(or 200-mesh) insize is preferred. The powder samples were placed into sample holders or onto the sample surfaces. Packing of fine powder into a sample holder is carried out as follows:

1. the samples were smeared uniformly onto a glass slide, assuring a flat upper surface
2. the samples were packed into sample containers
3. the samples were then sprinkled on double sticky tape

After this, the samples were then charged into the diffractometer. The intensity of diffracted X-rays is continuously recorded as the sample and detector rotate through their respective angles. A peak in intensity occurs when the mineral contains lattice planes with d-spacings appropriate to diffract X-rays at that value of θ . Although each peak consists of two separate reflections ($K\alpha_1$ and $K\alpha_2$), at small values of 2θ the peak locations overlap with $K\alpha_2$ appearing as a hump on the side of $K\alpha_1$. Greater separation occurs at higher values of θ . Typically these combined peaks are treated as one. The 2λ position of the diffraction peak is typically measured as the center of the peak at 80% peak height.

3.11 Scanning Electron Microscopy

A few tenths of a gram of the samples were obtained, as pure as possible and grinded to a fine powder less than 10×10^6 m (or 200-mesh) in size. The powder samples were placed on an aluminum holder stub using a double sticky carbon tape. The samples were then insulated with gold and electrically grounded. Then the samples were completely dried in the oven at 60°C for at least 3 hours depending on the sample conditions. The rule of thumb is that it is better to leave them overnight in the drying oven. The dried samples were then charged into the scanning electron microscope to view the morphology at different magnification.

CHAPTER FOUR

RESULTS AND DISCUSSION

4.1. Characterization of the Synthesized Photocatalysts

X-ray spectrometry, X-ray diffraction, Scanning electron microscopy, Specific surface area analyses and the Point of zero charge techniques were all used for the characterization.

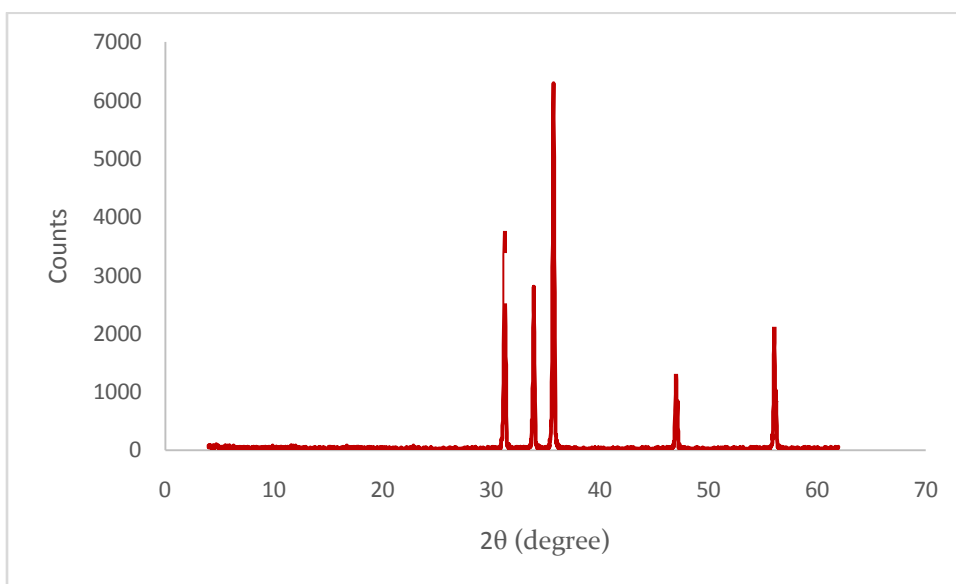
4.1.1. Chemical compositions of raw kaolin, beneficiated kaolin and mullite

Table 4.1 presents the chemical composition of the raw kaolin, beneficiated kaolin and the mullite produced. The Si/Al ratio of the raw clay which was initially 1.90 decreased slightly by 2.4% after beneficiation. The decrease in the Si/Al ratio could be attributed to washing away of silica during the beneficiation process. There was no appreciable reduction in, CaO, CuO and TiO₂. Nevertheless, some appreciable reductions were observed in the K₂O, Na₂O, MgO and trace elements before and after beneficiation. The reductions likely occurred as result of washing off of soluble salts during the beneficiation process. It is worth noting that Fe₂O₃ had rather increased after the beneficiation; it was not clear what was responsible for the increment, however, the same trend have been reported for Kankara clay by other researchers (Otu^{et al.}, 2013). The loss of ignition(L.O.I or others) of the raw kaolin was 11.85 wt%, it increased 12.20wt% after beneficiation. The increase after beneficiation could be attributed to increase in clay content of the kaolin resulting from washing away of impurities.

Content	Raw kaolinite wt %	Beneficiated kaolinite clay wt %	Mullite wt %
Al ₂ O ₃	28.49	29.40	45.30
SiO ₂	56.29	55.20	51.20
K ₂ O	1.10	0.51	0.20
Na ₂ O	0.14	0.04	NA
CaO	0.29	0.27	0.18
MgO	0.61	0.04	NA
TiO ₂	0.24	0.14	0.08
MnO	0.008	0.006	0.015
V ₂ O ₅	0.017	-	0.0088
Cr ₂ O ₃	0.044	0.024	0.012
BaO	0.16	0.09	0.01
ZnO	0.014	0.002	NA
Fe ₂ O ₃	0.537	0.65	0.921
Eu ₂ O ₃	0.12	0.11	0.008
NiO	0.02	0.011	0.016
CuO	0.043	0.032	0.0086
Ga ₂ O ₃	0.027	0.019	0.009
Others	11.85	12.20	-
Total	100	98.74	97.97

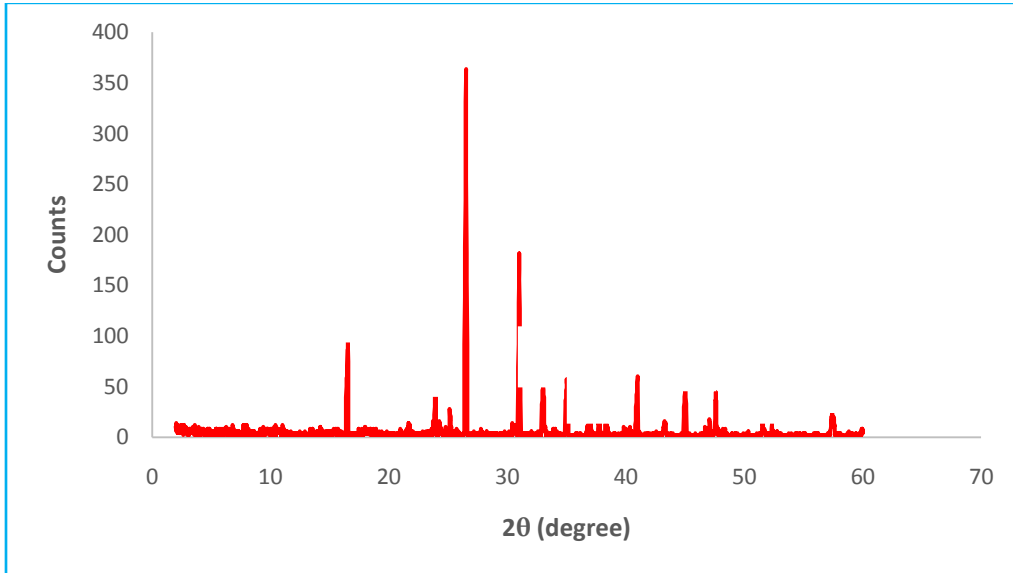
4.1.2 XRD analysis of the synthesized photocatalysts

Figure 4.1 shows the XRD patterns of the synthesized ZnO from thermal decomposition of basic zinc carbonate. The XRD pattern was characterized by some dominant peaks at high and low intensity with Bragg's angles of 31.3° , 34.8° , 35.7° , 47.1° and 56.1° as reported by Huttera *et al.*, (2013). This is also in agreement with the powder diffraction standard data (JCPDS No. 36-1451). The reflection peaks corresponding to the planes (100), (002), (101), (102), (110) confirms the hexagonal wurtzite structure of ZnO.



The dominant peaks detected correspond to the peaks of zincite, which shows that the thermal decomposition of ZnCO_3 into ZnO at 1200°C had minimal impurities as reported by Ghaffarian *et al.*,(2011). The ZnO crystallite diameter size D was calculated using the

Debye-Scherrer's formula given by equation 2.20. The particle size and specific surface area (SSA) of the synthesized ZnO samples were 54.23nm and 86.2m²/g respectively.



XRD patterns of mullite sintered at a temperatures of 1200 °C for 2 h using the heating rate of 10 °C/ min is given in Figs. 4.2. The XRD analysis showed some amount of impurities (quartz) and Braggs angles of 16.5⁰, 26⁰, 31⁰, 33⁰,35⁰,41⁰45⁰,47⁰,59⁰ which is in agreement with the powder diffraction standard data (JCPDS No. 15-0776) and reported literature. However there were minimal amount of impurities reported by other researchers, this can be attributed to geographical location and soil formation(Aksel and Kalem tas, 2004)

4.1.3 Scanning Electron Microscopy (SEM) Analysis

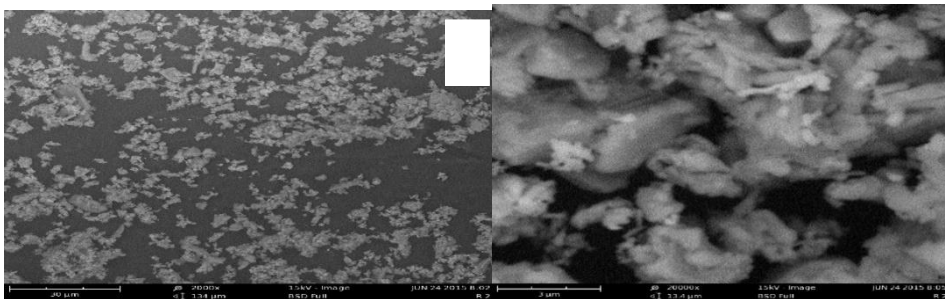
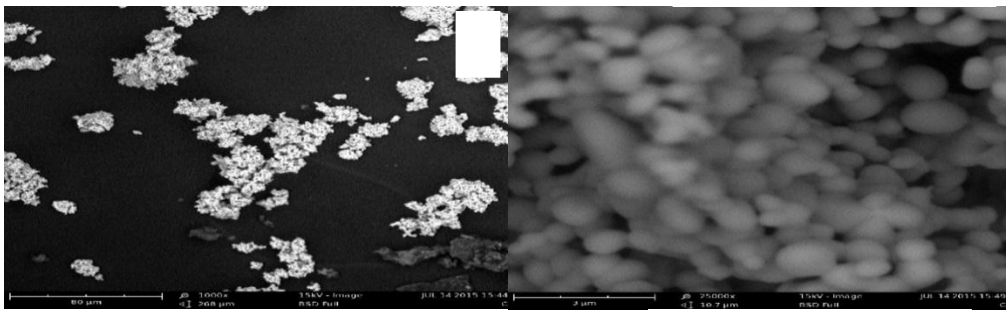
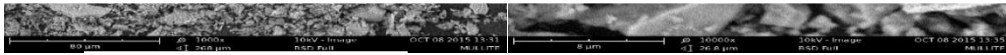
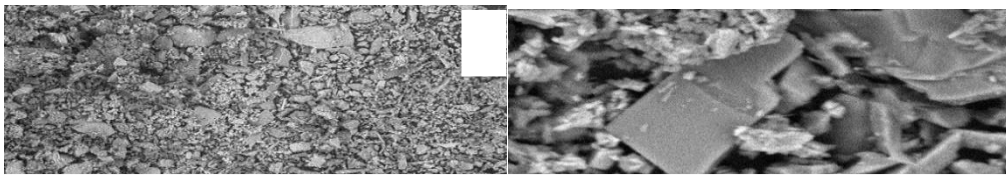
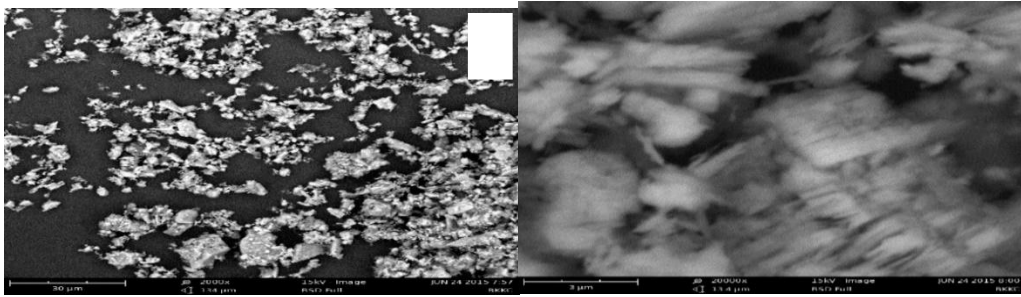


Plate 1a show the SEM images of beneficiated Kankara kaolin, scanned at 2000 and 20000 magnifications. The platelet structure of kaolinite clay reported in the literature (Abo-El-Enein, *et al.*, 2013; Bergaya, 2013) which normally portrays booklets morphology could be observed. The booklet morphology consisting of platelet sheets of kaolinite mineral as reported in the literature, becomes clearer at high magnification only. Plate 1b shows the SEM images for mullite samples sintered at 1200 °C for 2h. This SEM analyses images portrays particles with varying crystallite sizes of Mullite, beside some impurities of quartz in the sintered substrate as reported in literature (Tucci *et al.*, 2007; Oliverira *et al.*, 2002; Lee, 1998). The thermal decomposition of the kaolinite fired at 1200°C depicts some typical features of amorphous regions in the physical transformations as also seen in plate 1b. This could be attributed insufficient heat penetration through sample and high heating rate as reported in literature (Lee *et al.*, 2008; Romero *et al.*, 2006; Chen *et al.*, 2000). It is clearly observed that at a higher magnification plate (1b), the presence of a plate-like structure (mullite) is seen. Plate 1c represents the SEM image of synthesized ZnO particles at different magnifications. These image shows that the synthesized ZnO have spherical morphology with crystallite size of less than 1µm. These image substantiate the approximate spherical shape of ZnO, and most of the particles exhibit some faceting as reported in literature (Wang, 2004; Gao *et al.*, 2005; Gupta *et al.*, 2006). The measured surface area of the synthesized ZnO (86.2m²/g) is in agreement with reported works in literature (Polarz *et al.*, 2005; Jiu *et al.*, 2003) which gave the range between 11m²/g to 202m²/g depending on the mode of preparation. Also the high sintering temperature (1200⁰C) used in the syntheses resulted in having highly crystalline ZnO (Zhou *et al.*, 2007; Zhai *et al.*, 2008).

Plate 1d shows the SEM images for 20-ZnO/mullite sample sintered at 1200 °C for 2h. The attachment of ZnO particles into clay support change surface profile of mullite as reported in literature (Ma *et al.*, 2009; Modirshahla *et al.*, 2009). ZnO particles are uniformly deposited on the surface of mullite. It is found that ZnO dispersion was followed by reducing surface area of mullite (202.2 m²/g).

4.1.4. Specific Surface Areas of the Synthesized Photocatalysts

The specific surface areas of the synthesized ZnO, mullite and the ZnO/mullite measured using the sear's method are shown in Table 4.2. As can be seen in the table, the specific surface area of the unsupported Mullite is 202.2 m²/g. When ZnO was loaded on mullite the specific surface area of the composite decreased with increase in the ZnO loading. It has been reported that the specific surface area of the photocatalysts mostly decreases with increase in the molar ratio of the active component on the support material (Kostedt *et al.*, 2010).

Table 4.2 Specific surface areas of the synthesized ZnO and various ratios of ZnO/Mullite.

Photocatalysts	Specific Surface Area (m ² /g)
ZnO	86.2
10wt% ZnO/mullite	147.8
20wt% ZnO/mullite	144.6
30wt% ZnO/mullite	106.2
40wt% ZnO/mullite	96.6
50wt% ZnO/mullite	91.7
Mullite	202.2

4.1.5 pH at point of zero charge of the photocatalyst

The pH at point of zero charge (pH_{PZC}) of synthesized ZnO and the mullite supported ZnO are presented in Table 4.3. The measured pH at point of zero charge of synthesized ZnO via impregnation method was 8.7, which is close to the values of 8.5 – 9.3 reported in the literature (Fatehah *et al.*, 2014; Li *et al.*, 2013; Zhang *et al.*, 2008). pH at point of zero charge (pH_{PZC}) determines the pH where the surface charge of the material is zero or neutral. Above this pH_{PZC} (8.7), the ZnO surface is negatively charged due to the formation of O^{2-} on the surface while below 8.7 the surface charges of ZnO particles are positively charged as a result of formation of Zn^{2+} . For the ZnO/mullite composites, it was observed that the pH values increased from 10 wt% ZnO/Mullite to 50 wt% ZnO/Mullite which represent a shift towards the pH at point of zero charge of SiO_2 .

Table 4.3. pH at zero of point charge of the photocatalysts

Photocatalysts	pH _{pzc}
ZnO	8.7
10 wt% ZnO/Mullite	6.3
20 wt% ZnO/Mullite	6.8
30 wt% ZnO/Mullite	7.3
40 wt% ZnO/Mullite	7.8
50 wt% ZnO/Mullite	8.2

This indicates that the attachment of silica on the bare ZnO surface. However, there are insufficient reported literatures on the pH_{PZC} of various proportions of the composites but it can be deduced from Table 4.3 that silica layer had a great influence on altering the pH_{PZC} of ZnO which led to the increase in the pH values as the ZnO loading increases (Dong *et al.*, 2015).

4.1.6 Preliminary evaluation of photocatalytic activity of the synthesized ZnO and ZnO/mullite composites.

Preliminary evaluations of photocatalytic activity of ZnO and ZnO/Mullite composites were carried out on model compounds (Methylene blue) in line with the International Standard

Organization (ISO-10678:2010) and is reported various literatures (Qaradawi and Salman 2002; Wang *et al.*, 2004). This evaluation was in order to determine the photocatalytic activities of ZnO and relative mullite supported ZnO. Photocatalytic evaluation of ZnO and varying proportion of ZnO/Mullite (10-ZnO/mullite, 20-ZnO/mullite, 30-ZnO/mullite, 40-ZnO/mullite and 50-ZnO/mullite) were carried out. These evaluations were carried out under visible light illumination at various time interval while the degradation processes were monitored. Figure 4.3 shows the effect of irradiation time on the photocatalytic decolourisation of methylene blue. The decolourisation efficiency increased with increase in irradiation time up to about 60 min. At the initial stages of the decolourisation process, there were abundance of active sites on the photocatalyst surfaces. Hence, it should be expected that the photocatalytic reactions will be fast during these early stages. Similar observations have been reported by other researchers (Umoren *et al.*, 2013; Liu *et al.*, 2014).

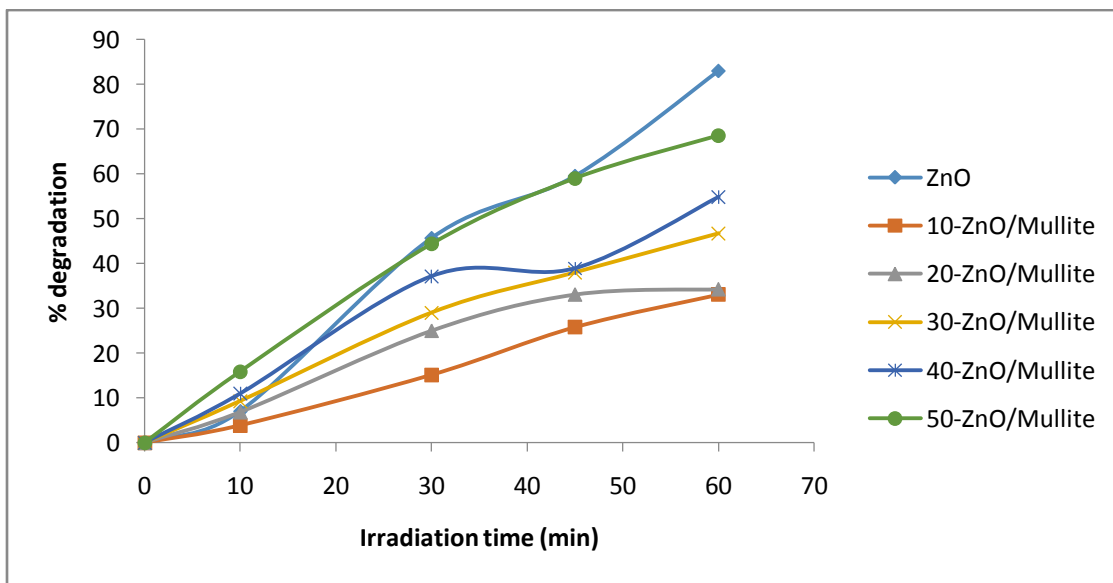


Figure 4.3: Photocatalytic degradation of MB using ZnO and varying proportion of ZnO/Mullite composites under visible light irradiation

The kinetic parameters of photocatalytic degradation of MB in aqueous solution with ZnO and The kinetics of photocatalytic degradation of MB is usually described by the pseudo-first order approximation of the Langmuir Hinshelwood (L-H) kinetic model (Equation. 2.34). The plot of $\ln C_0/C$ against time (Figure 4.4) resulted in a linear relationship from which the values of the apparent rate constants (k_{app}) were determined. The pseudo first order rate constants calculated from the plot are given in Table 4.3 for each photocatalyst studied. The straight line plots as well as the high values of R^2 obtained showed that the pseudo first order equation was able to describe the kinetics of the process. The values of the k_{app} increases with increase in the ZnO content of the composite. This can be attributed to the increase in available active sites on the surfaces of the catalyst. Similar observations were reported by Eren and Acar (2006).

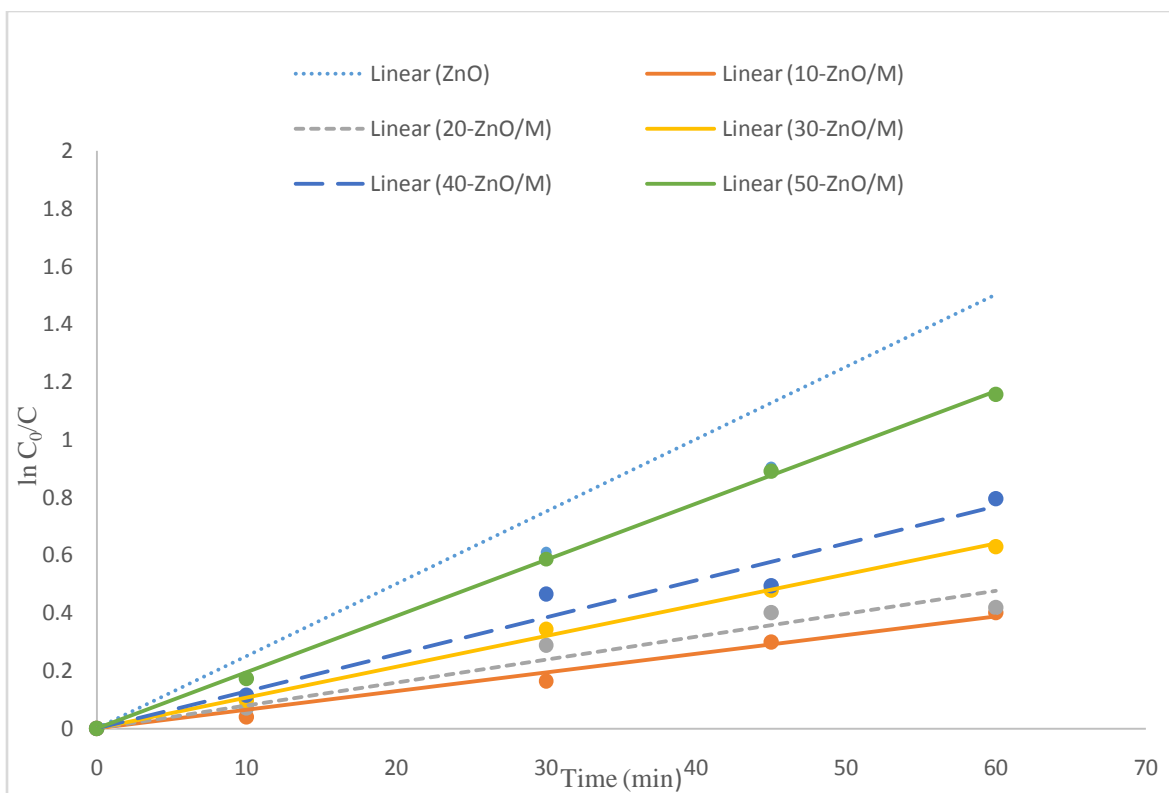


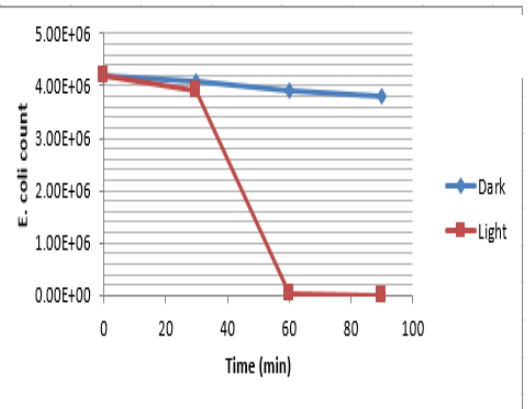
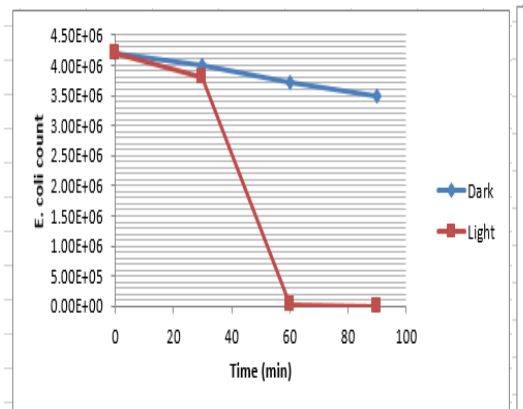
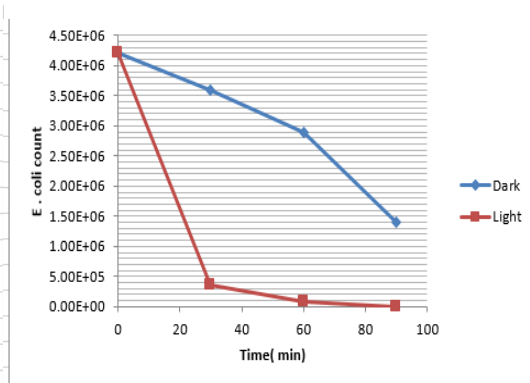
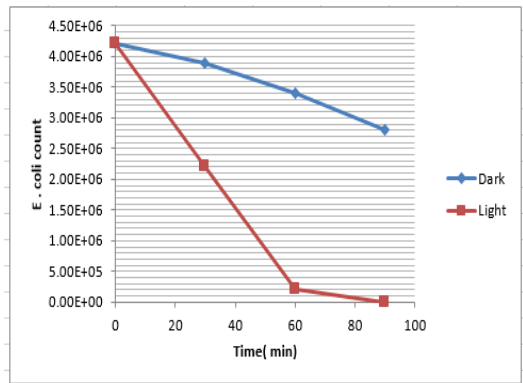
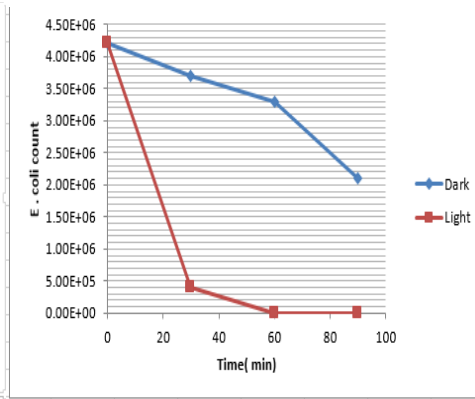
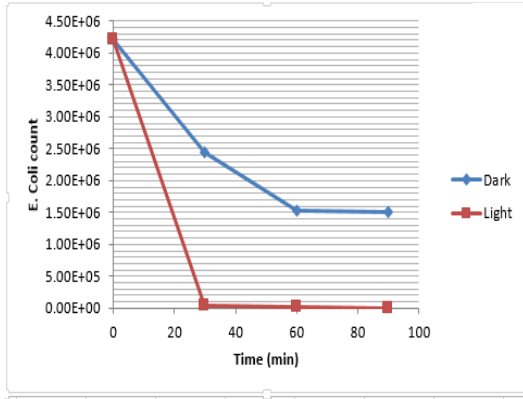
Figure 4.4: Pseudo first order kinetic plot for the solar photocatalytic degradation of methylene blue using the synthesized ZnO/Mullite composites

Table 4.4: Values of $K_{app}(\text{min}^{-1})$ and R^2 for MB degradation using ZnO and ZnO/Mullite composites

Sample	Rate constant, $k_{app} \times 10^{-3} (\text{min}^{-1})$	R^2
ZnO	24	0.91
10- ZnO/Mullite	6.4	0.99
20- ZnO/Mullite	7.8	0.96
30- ZnO/Mullite	10.7	0.99
40-ZnO/Mullite	12.9	0.94
50-ZnO/Mullite	19.4	0.99

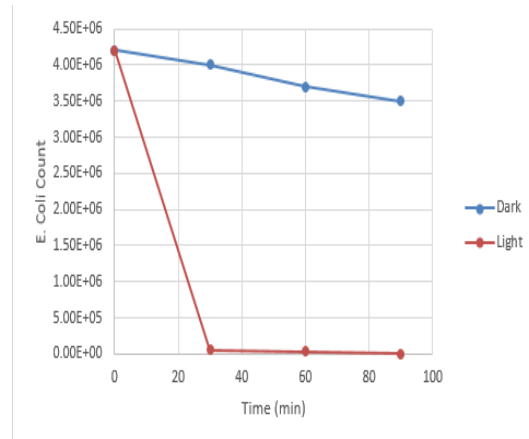
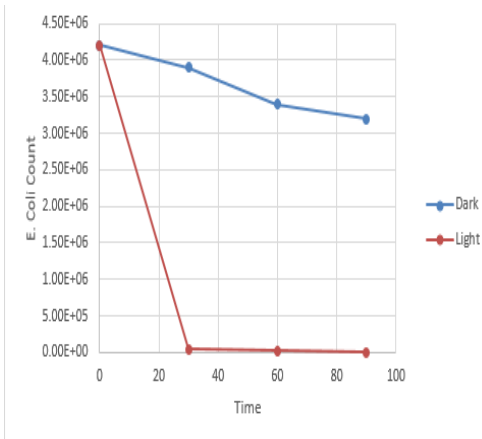
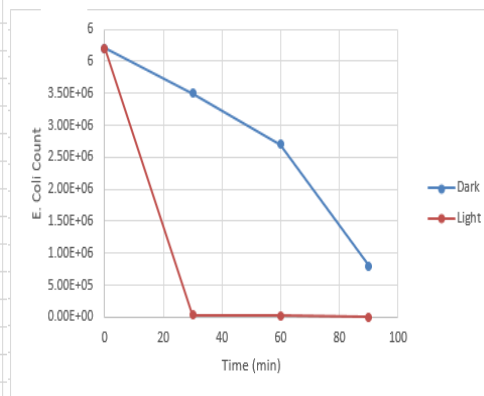
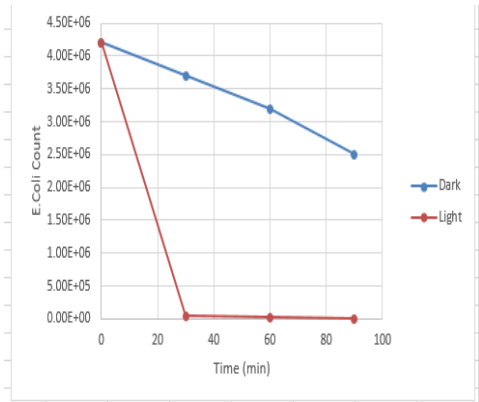
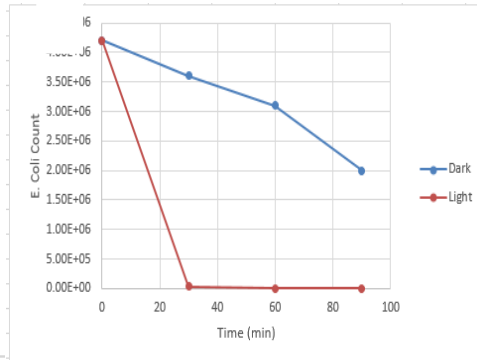
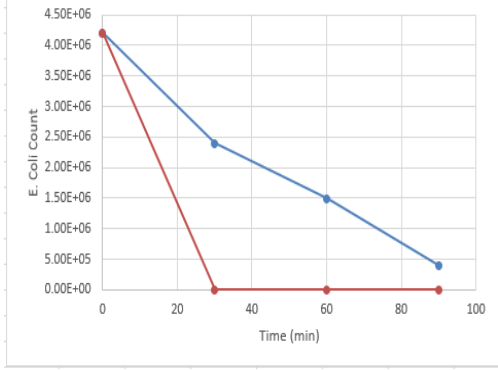
4.2 Photocatalytic Inactivation of *E.coli* and *S.entericain* Water

The results of the photocatalytic inactivation are presented in Figure 4.5, 4.6, 4.7, 4.8. More than 90% bacterial inactivation was achieved by the ZnO/mullite composite system under visible light irradiation. ZnO as powerful oxidizing agent, oxidizes the bacterial cell wall together with internal contents, and consequently cause cell death. Supporting ZnO on mullite increases the surface area of ZnO making it more expose to visible light. The ZnO is sensitive to UV tail that exists in the visible light. Thus the ZnO absorbs the UV tail and behaves as photo-catalyst with good catalytic activity causing up to ~ 98% inactivation. This enhancement observed in the ZnO/mullite is attributable to the extended and elevated absorption in the visible range and the reduction in the carrier recombination due to effective charge separation in accordance with interfacial model for the ZnO/mullite systems. Figure 4.5 gives a representation of *E.coli* inactivation using 1g of the synthesized ZnO and ZnO/mullite composite.

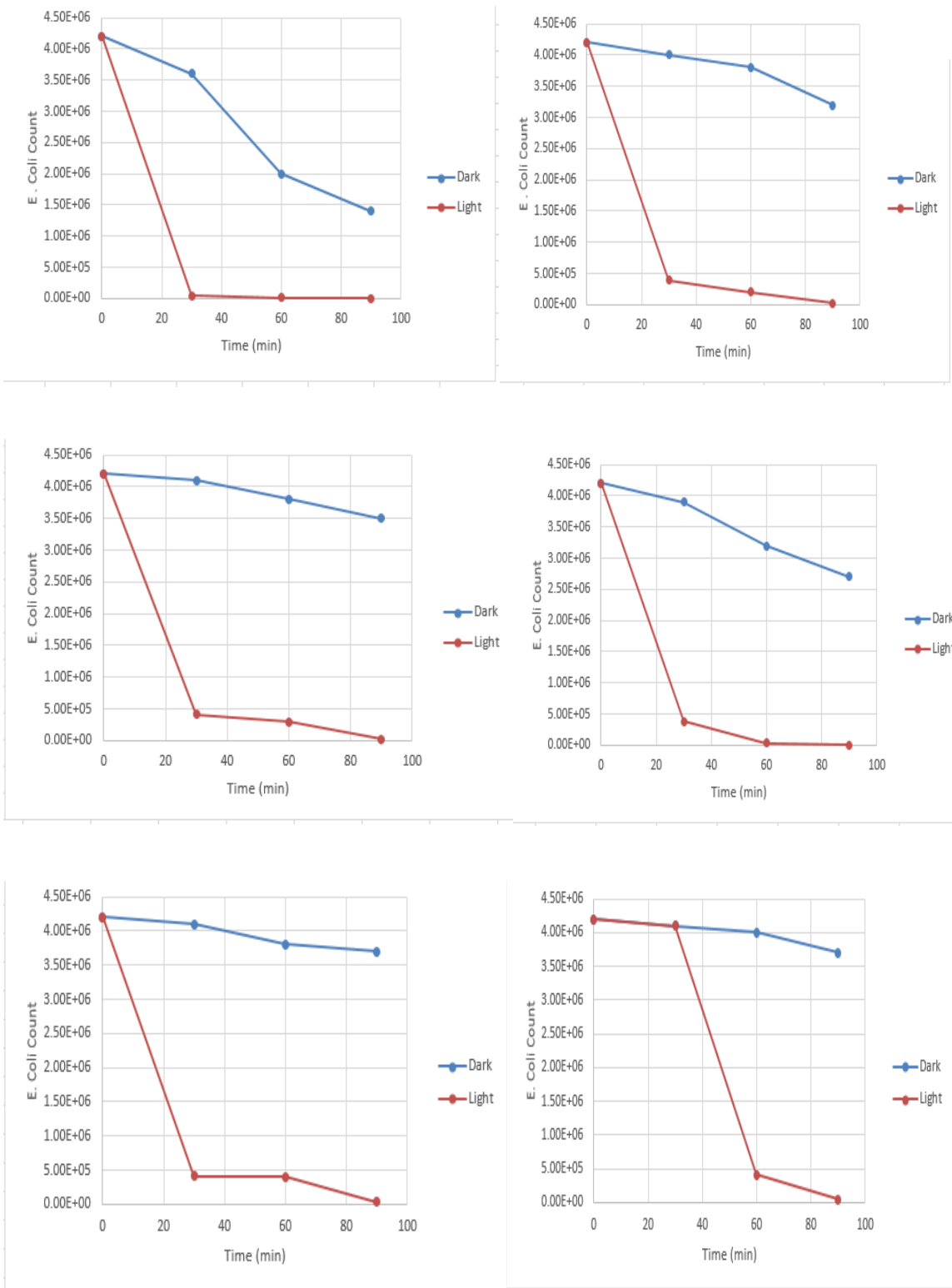


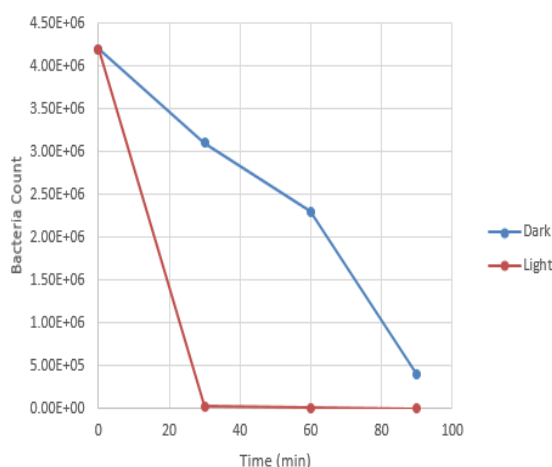
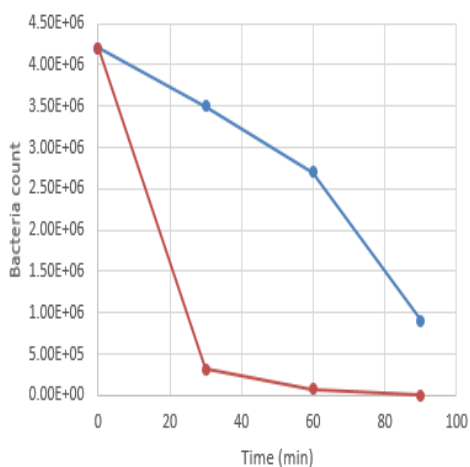
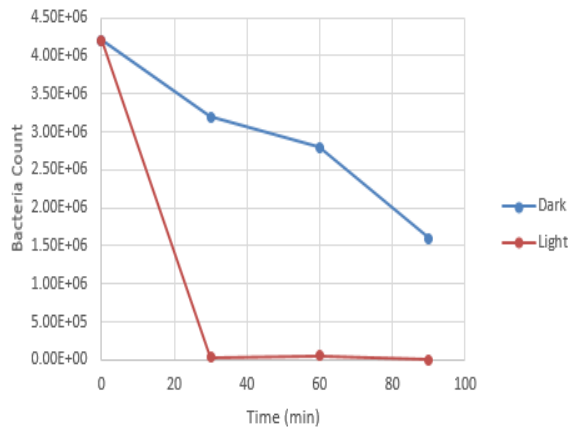
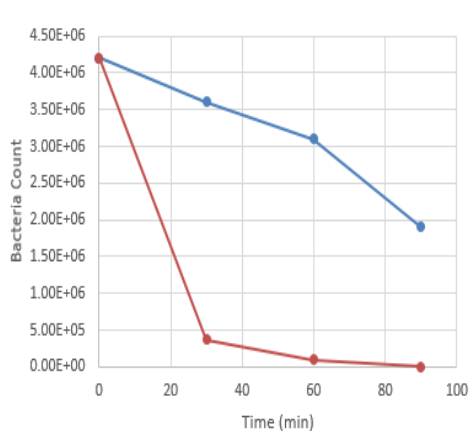
4.2.1 Effect of photocatalyst concentration on efficiency

For economic disinfection of contaminated water, the optimum amount of photocatalyst necessary for efficient inactivation was investigated here. Inactivation percent increased with increasing the added weight of the photocatalyst until a maximum efficiency was observed at a given catalyst weight (0.5 – 2.0g) this observation was also reported by Is(2012). Increasing the amount of the photocatalyst provides higher surface area and more active sites for the adsorption and inactivation reaction and makes more utilization for the incoming light that transmitted through the reaction medium in the photo-catalytic reaction. Therefore, higher percent of inactivated bacteria was achieved with more photocatalyst. However, increasing amount of the photocatalyst more than the 1.5 g/L brings about turbidity in the reaction medium, which shields off incident light. This leads to decrease in measured photocatalyst efficiency and bacterial inactivation percentage as shown in figure 4.5, 4.6, 4.7 and 4.8.



Both the synthesized ZnO and ZnO/mullite photocatalyst showed high percentage of inactivation (Figure: 4.5, 4.6, 4.7 and 4.8). The system was more efficient in the light phase when compared with the dark phase. Inactivation range of between 90 to 98% was achieved using both ZnO and ZnO/mullite photocatalyst within 30- 90 min depending on the generation of reactive hydroxyl radicals on the surfaces of the photocatalyst. This behavior was noticed in the 2.0g photocatalyst concentration both for ZnO and ZnO/mullite catalysts even in the dark as shown in Figure 4.7. Various literature reports emphasized parallel behaviors (Paddock *et al.*, 1999; Brayner *et al.*, 2006; Tayel *et al.*, 2011]. ZnO/mullite photocatalyst have higher surface area and more active sites. More bacterial cells adsorbed on the catalyst surface and more percent of bacteria inactivation is achieved. The amount of the dispersion particles, per volume in the reaction medium, increases with decreasing ZnO particle size. This enhances photon absorbance and H₂O adsorption on the surface.

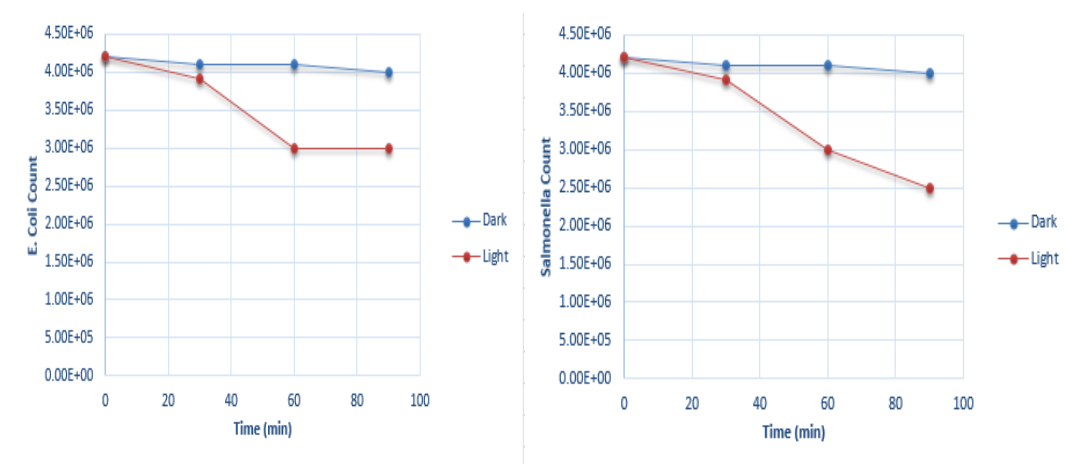




4.2.2 Effect of control experiments on bacterial inactivation

Control experiments were conducted in the absence of catalyst, absence of light, or absence of both (Figure 4.9). Some bacteria were affected with photolysis, in the absence of any photocatalyst type, showing up to 35% loss due to the visible light irradiation. Despite the need of bacteria for light in their life and growth, it may be harmful for them. Visible light

contains UV tail that affects the bacterial cell and causes mutations (changes in DNA sequence). The *E. coli* and *S. entericabacteria* are known to be especially sensitive to UV irradiation (Oteiza *et al.*, 2005). During the dark experiment, the slight inactivation recorded in the bacterial concentration, were due to bactericidal activity of Zn^{2+} ions that could accumulate in the cell membrane and causes disruption of the membrane (Atmaca *et al.*, 1998). Zinc penetrates through the cell membrane and inhibits nutrient uptake and interferes with proton transfer (Paddock *et al.*, 1999). Mullite itself didn't affect *E. coli* and *S. entericabacteria* (Figure 4.9). It is reported in literature that most support material incorporated in photocatalysis enhances the surface area of the active substance only.



4.2.3 Effect of bacteria concentration on photocatalyst efficiency

At low bacterial concentrations, increasing the photocatalyst concentration increased the inactivation percent (Table 4.5). At higher concentrations, increasing bacterial concentration lowered inactivation percentage as when compared with lower bacterial concentration. When bacteria concentration increases more bacterial cells are adsorbed on the catalyst

surface and so more bacterial cells are inactivated. That is why higher percentage of inactivation were recorded in most of the photocatalyst concentration used over time.

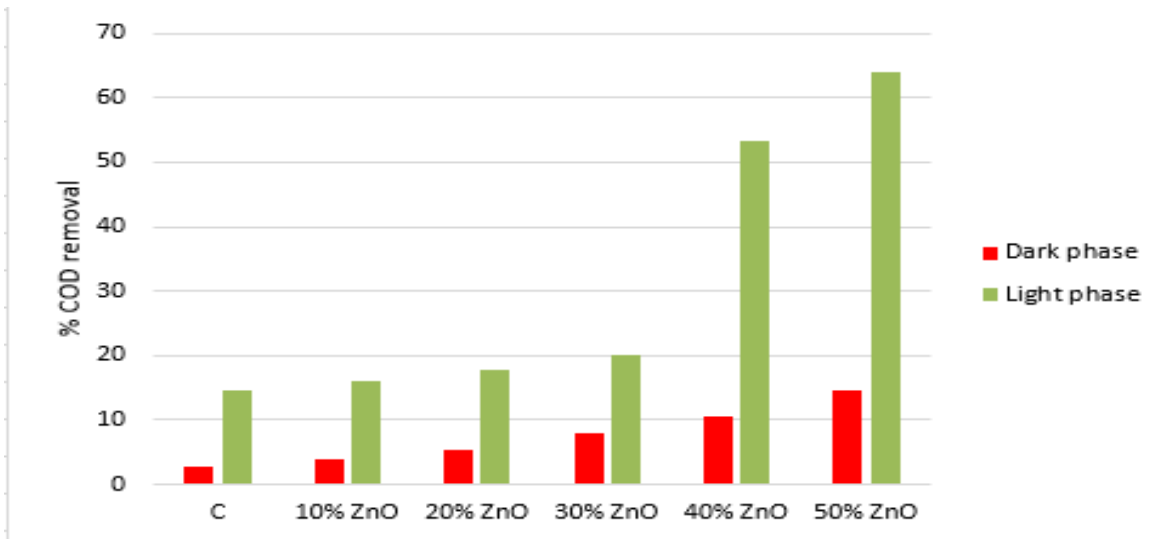
Table 4.5: Performance of ZnO/Mullite for inactivation of bacteria in Zaria raw water in the dark and under illumination for 90 min

Composition Initial cfu	Dark experiment cfu/ml 2×10^4	Photocatalytic exp cfu/ml 2×10^4
Mullite	2.0×10^4	$2. \times 10^3$
ZnO	367	0.00
10%ZnO/M	355	0.00
20%ZnO/M	350	0.00
30%ZnO/M	311	0.00
40%ZnO/M	230	0.00
50%ZnO/M	205	0.00

4.2.4 Photocatalytic treatment of Zaria dam raw water.

The COD value is a measure of all chemically degradable organic pollutants in water. The result of COD reduction of the Zaria dam raw water via photolysis adsorption in the dark and photocatalysis are presented in Fig. 4.11. It was found that irradiation of the raw water for 90 mins in the absence of photocatalysts (photolysis) showed no significant reduction in the COD, this indicates that the organic load of the sample irradiated without photocatalyst did not change drastically and the small change in the COD observed was due to the photochemical – oxidation of the organic compounds present in the raw water (Pelentridou *et al.*, 2009). Therefore, irradiation without photocatalyst was not sufficient to degrade efficiently the raw water. When the solution was exposed to visible light irradiation in the presence of ZnO and varied proportion of ZnO/mullite photocatalyst for 90 mins, an appreciable reduction in the COD (14- 64%). This is in agreement with work carried out by Vineetha *et al.*(2013) where an increase in the photocatalyst dosage resulted in 75%

reduction in the COD. Figure 4.12 evidently shows that 50 wt% ZnO/mullite photocatalyst synthesized has better photocatalytic performance than other photocatalysts synthesized in reference to the COD reduction.



4.3. Kinetic Study for *E.coli* inactivation and microbicidal photonic efficiency

The bactericidal activities of the synthesized ZnO and ZnO/Mullite samples were investigated by evaluating the inactivation of *E. coli* bacterium under dark and visible light irradiation. The results of the comparison of the photocatalyst are depicted in Fig. 4.11. The Gram negative bacterium *E.coli* can be almost completely inactivated within 90 min with mixed ZnO/mullite photocatalysts under visible light irradiation. The decrease of the cfu count on an agar plate was used for evaluation of bactericidal activities. The Chick–Watson model was applied as a disinfection kinetic model (Marugan *et al.*, 2008). The rate constant was calculated by plotting $\ln N/N_0$ against time (Fig. 4.12) where N and N_0 are survived and initial cfu count of *E.coli* under exposure. The rate constant values are given in Table 4.6. All the synthesized photocatalysts under irradiation samples showed high rate constant compared to the one in the dark. A small increase in rate constant observed in the 1 g/L compared to the other concentrations. The rate constants values are comparable with that in literature (Akhavan *et al.*, 2009; Ranjith *et al.*, 2011). This result clearly indicates the role of developed photocatalyst in the inactivation process.

Photocatalyst (g/l)	Rate constant min^{-1} Light	Rate constant min^{-1} Dark	R ²
0.5	0.1216	0.0140	0.977
1.0	0.1900	0.0144	0.968
1.5	0.0884	0.0055	0.989
2.0	0.0105	0.0046	0.936

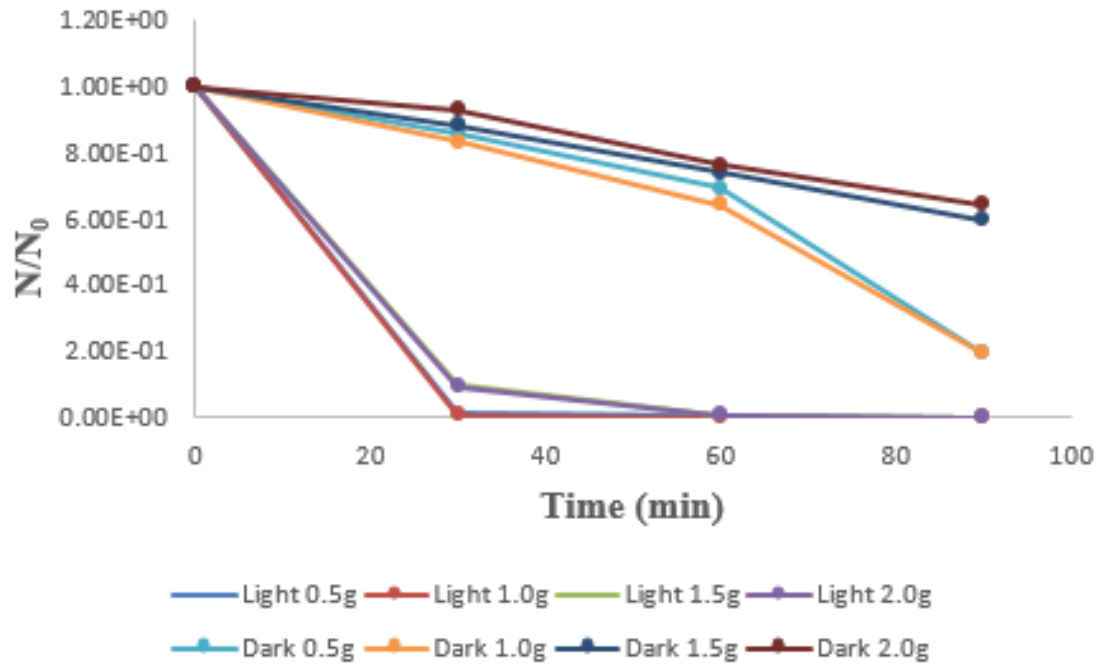


Figure 4.11: *E. coli* inactivation spectra of ZnO/mullite samples

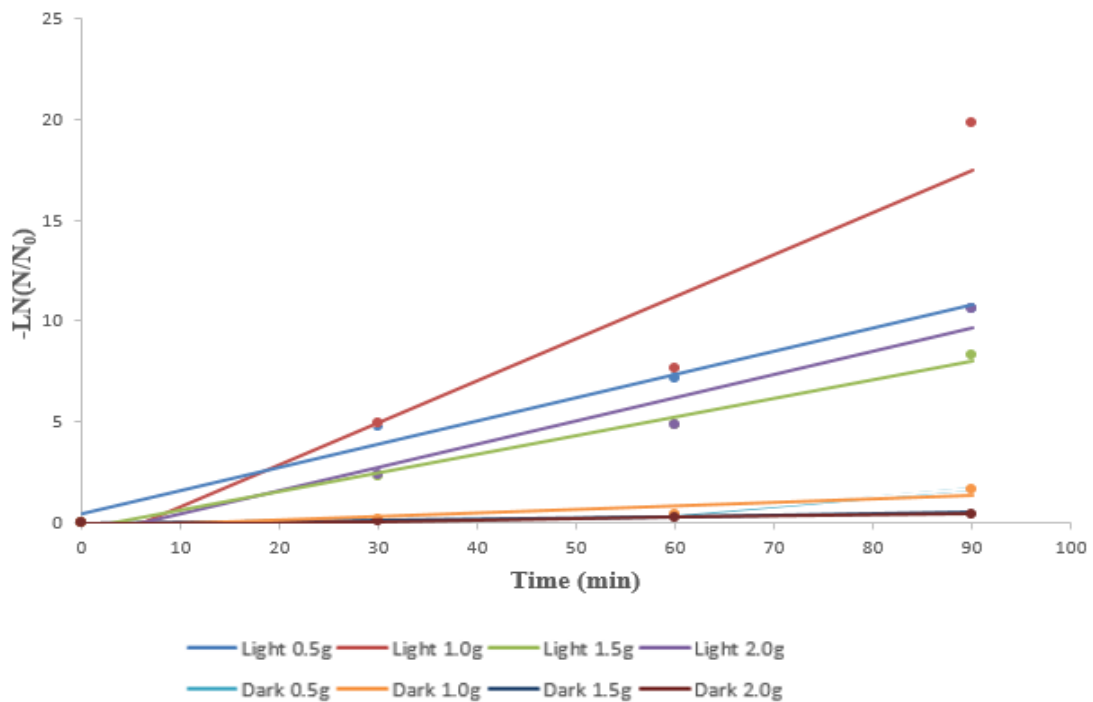


Figure: 4.12 Disinfection rate constant calculation spectra of ZnO/mullite samples

CHAPTER FIVE

CONCLUSIONS AND RECOMMENDATIONS

5.1 Conclusions

The following conclusions were made based on the results obtained in this research:

1. ZnO and its support :10-ZnO/mullite, 20-ZnO/mullite, 30-ZnO/mullite, 40-ZnO/mullite and 50-ZnO/mullite were synthesized by impregnation method and characterized using XRD,XRF, SEM, pH_{pzc} and surface Area Analysis.
2. The preliminary Photocatalytic evaluation showed that the photodegradation of MB using the synthesized ZnO was 82.97% while 50-ZnO/mullite support exhibit the highest photodegradation of 68.57% among the ZnO/mullite supports. This activity decreases with decrease in ZnO content.
3. The experimental data for the photodegradation of MB obtained followed the pseudo first order kinetic model
4. Anchoring the ZnO on mullite layer as a support shows its potential on altering the pH_{pzc} of ZnO.
5. The 1 g/L and the 30-ZnO/mullite support gave a better performance in the inactivation of *E.coli* and *S.enterica*.
6. The 1g/L, 30wt%-ZnO/mullite sample showed high rate of bacterial inactivation among the concentrations compared.
7. The efficacy of the ZnO/mullite in *E.coli* inactivation of Zaria raw water under visible light illumination was high (complete inactivation within 90 min).

8. The percentage COD reduction of Zaria dam raw water was 64 using the 50-ZnO/mullite support.

Recommendation

1. The ZnO/mullite photocatalyst should be tested against other types of bacteria (e.g. gram positive bacteria) and other microorganism
2. The ZnO/mullite photocatalyst should be tested on different chemical pollutants such as fertilizer, pesticides, drugs and other water pollutant.
3. The ZnO should be anchored on different supports such as activated carbon and sand to compare the inactivation processes.
4. Other methods for ZnO preparation should be considered since the preparation methods has influence on the particle size and studying the efficiency.
5. The photocatalytic activity against bacteria on longer time intervals should studied.

REFERENCES

- Abo-El-Enein, S. A., Heikal, M., Amin, M. S. and Negm, H. H., Reactivity of dealuminated kaolin and burnt kaolin using cement kiln dust or hydrated lime as activators. *Construction and Building Materials*, 47: 1451–1460,(2013).
- Ahmed, A. S. Properties of Kaolin and Methods of Beneficiation: Proceedings of the First Nigerian Conference on Zeolite, Organized by PTDF Professorial Chair in Chemical Engineering, Ahmadu Bello University, Zaria, Held at Institute of Development Research, ABU, Zaria, 1:1–17, (2008).
- Ajayi, A. O. Development of Large Pore Zeolite from Kankara and Elefun Kaolinite. Unpublished Ph. D Dissertation, Department of Chemical Engineering, Ahmadu Bello University, Zaria. (2012).
- Ajayi, A. O., Atta, A. Y., Aderemi, B. O. and Adefila, S. S., Novel Method of Metakaolin Dealumination Preliminary Investigation. *Journal of Applied Sciences Research*, 6(10): 1539-1546, (2010).
- Akhavan, O. Abdolahad, M. Abdi, Y. Mohajezadeh, S.Synthesis of titania/carbon nanotube heterojunction arrays for photoinactivation of *E.coli* in visible light irradiation, *Carbon* 47, 3280–3287, (2009).
- Akhtar, T. and Alam, M.Synthesis and Characterization of Zinc Oxide Nanoparticles via a Novel Reverse-Micellar Route, *Internation Journal of Science & Research* 3 1362-1367, (2014).
- Asahi, R. T. Morikawa, T. Ohwaki, K. Aoki, and Y. Taga, “Visible-light photocatalysis in nitrogen-doped titanium oxides,”*Science*, vol. 293, no. 5528, pp. 269–271, 2001.
- Asbury J. B., Anderson N. A., Hao E., Ai X. & Lian T. Parameters Affecting Electron Injection Dynamics from Ruthenium Dyes to Titanium Dioxide Nanocrystalline Thin Film. *Journal of Physical Chemistry B*107, 7376–7386 (2003).
- Atmaca, S. Gul, K. and Cicek,R. “The Effect of Zinc on Microbial Growth”, *Turkish Journal of Medical Sciences*, **28** (1998) 595-597.
- Bard, A.J *Science* 207, 139, 1982
- Barret, E. P. Joyner, L. G. and Halenda, P. P. The Determination of Pore Volume ad Area Distributions in Porous Substances. I. Computations from Nitrogen Isotherms..*Journal of the American Chemical Society*. 73, 373-380, (1951).
- Bartsch, M. Saruhan, M. Schmucker, H. Schneider, Novel low-temperature processing route of dense mullite ceramics by reaction sintering of amorphous SiO₂-coated g-

- Al₂O₃particle nanocomposites, *Journal of the American Ceramic Society*. 82. 1388-1392, (1999).
- Belapurkar, A. D, P. Sherkhane and S. P. Kale, “Disinfection of drinking water using photocatalytic technique”, *Current Science.*, 91(2006).
- Bergaya, F. and Lagaly, G., “*Handbook of clay science*”. 2nd edition, 18-295, Amsterdam, Netherlands, Elsevier, (2013).
- Bitenc, M. Marinšek, M. and Crnjak Orel, Z. “Preparation and characterization of zinc hydroxide carbonate and porous zinc oxide particles,” *Journal of the European Ceramic Society*, vol. 28, no. 15, pp. 2915–2921, 2008.
- Brayner, R. Ferrari-Iliou, R. Brivois, N. Djediat, Sh. Benedetti, M. F. and Fievet, F. “Toxicological Impact Studies Based on *Escherichia coli* Bacteria in Ultrafine ZnO Nanoparticles Colloidal Medium”, *Nano Letters.*, 6.866-870, (2006).
- Brindley, G.W. Nakahira, M. The kaolinite-mullite reaction series: I, a survey of outstanding problems, *Journal of the American Ceramic Society*. 42. 311-314, (1959).
- Brindley, G.W. Nakahira, M. The kaolinite-mullite reaction series: II, metakalin, *Journal of the American Ceramic Society*. 42 314-318, (1959).
- Brindley, G.W. Nakahira, M. The kaolinite-mullite reaction series: III, the high-temperature phases, *Journal of the American Ceramic Society*. 42 319-323, (1959).
- Brindley, G.W. Nakahira, M. Kinetics of dehydroxylation of kaolinite and halloysite, *Journal of the American Ceramic Society*. 40. 346-350, (1957).
- Carty, W.M. Senapati, U. Porcelain – raw materials, processing, phase evolution, and mechanical behavior, *Journal of the American Ceramic Society*. 81. 3-20, (1998).
- Castelein, O., Guinebretière, R., Bonnet, J. P. & Blanchart, P., Shape, size and composition of mullite nanocrystal from a rapidly sintered kaolin, *Journal of the European Ceramic Society*, 21, 2369-2376, 2001.
- Cavalcante, P. M. T., Dondi, M., Ercolani, G., Guarini, G., Melandri, C., Raimondo, M., Rocha E. & Almendra, E. R., The influence of microstructure on the performance of white porcelain stoneware, *Ceramics International*, 30. 953-963, 2004.
- Chaudhuri, S. P. & Sarkar, P., Constitution of porcelain before and after heat treatment. Part II: Aspect ratio and size-distribution of mullite, *Journal of the European Ceramic Society*, 16. 851-855, 1996.

- Chaudhuri, S.P., Ceramic properties of hard porcelains in relation to mineralogical composition and microstructure: VI thermal shock resistance and thermal expansion. *Transactions of the Indian Ceramic Society*, XXXIV, 30-34, 1975.
- Chen, C. Y. & Tuan, W. H., Evolution of mullite texture on firing tape-cast kaolin bodies *Journal of the American Ceramic Society*, 85. 1121-1126, 2005.
- Chen, C. Y., Lan, G. S. & Tuan, W. H., Microstructural evolution of mullite during the sintering of kaolin powder compacts, *Ceramics International.*, 26, 715-720, 2000.
- Comer, J. Electron microscopy studies of mullite development in red kaolinites, *Journal of the American Ceramic Society*. 43. 378-384, 1960.
- Dong, H., Zeng, G., Tang, L., Changzheng, F., Zhang, C., He, X. and He, Y. An overview on limitations of TiO₂ – based particles for photocatalytic degradation of organic pollutants and the corresponding countermeasures. *Water Research*, 79 : 128 – 146. 1067–1075, (2015).
- Edomwonyi-Otu, L. C., Aderemi, B. O., Ahmed, A. S., Coville, N. J. and Maaza, M., Influence of Thermal Treatment on Kankara Kaolinite. *Opticon1826*, 15(5): 1-5, 2013.
- Fabrega, A.; Vila, J. "Salmonella enterica Serovar Typhimurium Skills to Succeed in the Host: Virulence and Regulation". *Clinical Microbiology Reviews* 26 (2): 308–341, (2013).
- Fatehah Mohd Omar, Hamidi Abdul Aziz, Serge Stoll. Aggregation and disaggregation of ZnO nanoparticles: Influence of pH and adsorption of Suwannee River humic acid. *Science of the Total Environment* 468–469, 195–201, (2014).
- Fatimah, Is. K. Wijaya and Narsito, Microwave Assisted Preparation of TiO₂/Al Pillared Saponite for Photocatalytic Phenol Photo-Oxidation in Aqueous Solution, *Arabian Journal of Chemistry*. (In Press).
- Fatimah, Is. Photocatalytic Antibacterial Activity of ZnO / Hectorite and ZnO / Montmorillonite hInt. *Journal of Chemical Sciences*: 10(3), 1341-1349, 2012
- Fatimah, Is. Wang, S. and Wulandari, D. ZnO/Montmorillonite for Photocatalytic and Photochemical Degradation of Methylene Blue, *Applied Clay Science.*, 53(4), 553-560, 2010.
- Fujishima, A. and Honda, K. "Electrochemical Photolysis of Water at a Semiconductor Electrode." *Nature* 238: 37-38, 1972.

- Fujishima, A., Zhang, X. and Trykb, D.A. Heterogeneous Photocatalysis: From water photolysis to applications in environmental cleanup. *International Journal of Hydrogen Energy*, 32: 2664-2672, (2007).
- Gao, P. X. Ding, Y.Mai, W. Hughes, W. L. Lao, C. and Wang,Z. L. “Materials science: conversion of zinc oxide nanobelts into superlattice-structured nanohelices,” *Science*, vol. 309, no. 5741, pp. 1700–1704, 2005.
- Gopal K, Tripathy SS, Bersillon JL, Dubey SP Chlorination byproduct, their toxicodynamics and removal from drinking water. *Journal of Hazardous Materials* 140 (1-2): 1-6, 2007.
- Hemrick, J.G. Peters,K. Advanced ceramic composites for molten aluminium contact applications, in: UNITECR’ 09 Proceedings, Salvador, Brazil, 2009.
- Hisao Suzuki, Masanori Shirmizu, Hidehiro Kamiya, Toshitaka and Minoru Takahashi, Preparation of fine mullite powders with high surface area by agglomeration control of alkoxide-derived precursor sol, *Advance Powder Technology* vol.8 No. 4 pp311-323, 1997.
- Hrenovic, J. Milenkovic, J. Daneu, N.Kepcija, R. N. and Rajic, N. Antimicrobial Activity of Metal Oxide Nanoparticles Supported onto Natural Clinoptilolite, *Chemosphere*, 88(9), 1103-1107, 2012.
- Hrenovic, J. Milenkovic, J. Ivankovic, T. and Rajic, N. Antibacterial Activity of Heavy Metal-Loaded Natural Zeolite, *Journal of Hazardous Materials*. 201-202, 260-264, 2012.
- Ibarra, M.N. Almanza, J.M. Cortes, D.A. Escobedo, J.C. Pech, M. Martinez, R. Effect of the addition of alkaline earth sulfates to mullite ceramics on the corrosion and wetting by Al-Mg alloy, *Journal of the European Ceramic Society*,. 35 2189–2194, 2015.
- JCPDS, Powder Diffraction File, Alphabetical Index, Inorganic Compounds, International Centre for Diffraction Data, Newtown Square, Pa, USA, 1977.
- Jeffrey, D. S. (Ed.), UNITECR_05: Proceedings of the Unified International Technical Conference on Refractories, November 8–11, Orlando Florida, USA, 9th Biennial Worldwide Congress on Refractories, 2015.
- Jina Choi. Development of visible-light-active photocatalyst for hydrogen production and environmental application, 2010.
- Kemper, Jerome M. Spencer S. Walse and William A. Mitch *Environmental Science and Technology*, 44 (4), 1224–1231, 2010,

- Koshy, P. Gupta, S. Sahajwalla, V. Edwards, P. Effect of CaF₂ on interfacial phenomena of high alumina refractories with Al alloy, *Metallurgical Materials Transactions. B* 39 603–612, 2008.
- Kostedt IV, W.L., Byrne, H.E. and Mazyck, D.W. A high surface area magnetic photocatalyst with controlled pore size. *Journal of Environmental and Sustainable Energy*, 29: 10–16, 2010.
- Krasner, SW, Scilimenti, M, Guo, YC, Hwang. C. Occurrence of a New Generation of Disinfection byproducts. *Environmental Science and Technology*. 40:23:7175, 2006.
- Kumar, P. Panchakarla, L. S. Bhat, S. V. Maitra, U. Subrahmanyam, K. S. and Rao, C. N. R “Photoluminescence, white light emitting properties and related aspects of ZnO nanoparticles admixed with graphene and GaN,” *Nanotechnology*, vol. 21, no. 38, Article ID 385701, 2010.
- Lee, E. J. & Iqbal, Y., Influence of mixing on mullite formation in porcelain, *Journal of the European Ceramic Society*, 21, 2583-2586, 2001.
- Lee, W. E., Souza, G. P., McConville, C. J., Tarvornpanich, T. & Iqbal, Y., Mullite formation in clays and clay-derived vitreous ceramics, *Journal of the European Ceramic Society*., 28, 465-471, 2008.
- Lee, W.E. Rainforth, W.M. *Ceramic Microstructures – Property Control by Processing*, Chapman & Hall, London, UK, 255-312, 1994.
- Li M, Lin D, Zhu L. Effects of water chemistry on the dissolution of ZnO nanoparticles and
- Liu, H. L. and Th. C. K. Yang, “Photocatalytic inactivation of *Escherichia coli* and *Lactobacillus helveticus* by ZnO and TiO₂ activated with ultraviolet light”, *Process Biochemistry*. 39:475-481, 2003.
- Liu, K.-C. Thomas, G. Caballero, A. Moya, S. de Aza, Time-temperature-transformation curves for kaolinite-₂-alumina, *Journal of the American Ceramic Society*. 77 1545-1552, 1994.
- Loosli F, Stoll S. Adsorption of TiO₂ nanoparticles at the surface of micron-sized latex particles, pH and concentration effects on suspension stability. *Journal of Colloid Science Biotechnology*; 1:113–21, 2012.
- Lu, A. Kiefer, H A. Schmidt, W. Schuth, F. *Chemistry of Materials*, 16, 2004.
- Ma. H, Williams PL, Diamond SA. Ecotoxicity of manufactured ZnO nanoparticles — a review. *Environmental Pollution*, 172:76–85, 2013.

- Mackenzie, J.K. Shuttleworth, R. A phenomenological theory of sintering, *Proceedings of Physical Society*. London 62 633-652, 1949.
- Magaña, S. M. Quintan, P. Aguilar, D. H. Toledo, J. A. Ngeles-Chávez, C. A Cortés, M. A. León, L. Freile-Peigrín, Y.López T.and Torres Sánchez,R.M. Antibacterial Activity of Montmorillonites Modified with Silver, *Journal of Molecular Catalysis*. A, 281(1-2), 192-199, 2008.
- Malachová, K. Praus, P. Rybková, Z. and Kozák, O. Antibacterial and Antifungal Activities of Silver, Copper and Zinc Montmorillonites, *Applied Clay Science*.,53(4), 642-645 2011.
- Manzo, S,Miglietta ML, Rametta G, Buono S, Francia GD. Toxic effects of ZnO nanoparticles towards marine algae *Dunaliella tertiolecta*. *Science of the Total Environment*; 445–446, 2013
- Marugan, R.V. Grieken, C. Sordo, C. Cruz, Kinetics of the Photocatalytic disinfection of *Escherichia coli* suspensions, *Applied Catalysis B: Environmental* 82. 27–36, 2008.
- McConville, C. J, Lee, W. E. & Sharp, J. H., Microstructural evolution in fired kaolinite, *Brit. Ceramic Transactions*., 97, 162-168, 1998.
- Meier,A. Javernick, D.A. Edwards, G.R.Ceramic–metal interfaces and the spreading of reactive liquids, *Journal of the minerals, metals and Materials Society*. 44–47, 1999.
- Meulenkamp EA. Size dependence of the dissolution of ZnO nanoparticles. *Journal of Physical Chemistry B*,Acad. Sci. USA, 96.6183–6188, 1999.
- Miyoshi, H. Ohno, H. Sakai, K. Okamura, O. and Kourai,H. Characterization and Photochemical and Antibacterial Properties of Highly Stable Silver Nanoparticles Prepared on Montmorillonite Clay in N-Hexanol, *Journal of Colloid and Interface Science*.,345(2), 433-441, 2010.
- Ng, H. T. Chen, B.J. Li et al., “Optical properties of single-crystalline ZnO nanowires on m-sapphire,” *Applied Physics Letters*, vol. 82, no. 13, pp. 2023–2025, 2003.
- Norton, F.H.Robert E. Krieger, *Fine Ceramics, Technology and Applications*, USA, (pp.27), 1978.
- Ohnishi, H. Matsumura, M. Tsubomura, M. Iwasaki M. Bleaching of Lignin Solution by a Photocatalyzed Reaction on Semiconductor Photocatalysts *Industrial and Engineering Chemistry Research*. 28, pp. 719–724, 1989.

- Okada, K. Otsuka, N. Characterization of the spinel phase from SiO₂-Al₂O₃ xerogels and the formation process of mullite, *Journal of the American Ceramic Society*. 69. 652-656, 1986.
- Okada, K. Otsuka, N. Osaka, J. Characterization of spinel phase formed in the kaolin-mullite thermal sequence, *Journal of the American Ceramic Society*. 69 c251-c253, 1986.
- Oliveira, M. Agathopoulos, S. Ferreira, J.M.F. Reactions at the interfase between Al₂O₃-SiO₂ ceramics with additives of alkaline-earth oxides and liquid Al-Si alloy, *Journal of Materials Research*. 17. 641-647, 2002.
- Ortiz-Covarrubias, K.E. et al., Synthesis of Al₆Si₂O₁₃-BaAl₂Si₂O₈-ZrO₂-based composites and their wettability by molten Al and an Al-Si alloy, *Ceramics International*. 2014.
- Oteiza, J.M. Peltzer, M. Gannuzzi, L. and Zaritzky, N. Antimicrobial efficacy of UV radiation on *Escherichia coli* O157:H7 (EDL 933) in fruit juices of different absorptivities, *Journal of Food Protection*. 68(1):49-58, 2005.
- Paddock, M.L. Graige, M.S. Feher, G. and Okamura, M.Y. "Identification of the proton pathway in bacterial reaction centers: inhibition of proton transfer by binding of Zn²⁺ or Cd²⁺". *Proceedings of the National Academy of Science*. 100. 102:7764-9 1998.
- Padmavathy and R. Vijayaraghavan, "Enhanced bioactivity of ZnO nanoparticles—an antimicrobial study", *Science Technology of Advance Materials*. 9 (7pp), 2008.
- Pan, X. Medina-Ramirez, I. Mernaugh, R. and Liu, J. "Nanocharacterization and bactericidal performance of silver modified titania photocatalyst", *Colloids and Surfaces, B*, 77 82-89, 2010.
- Papargyris, D., Cooke, R.D. Structure and mechanical properties of kaolin based ceramics, *British Ceramic Transactions* 95. 107-120, 1996.
- Pelentridou, K., Stathatos, E., Karasali, H. and Lianos, P. Photodegradation of the herbicide azimsulfuron using nanocrystalline titania films as photocatalyst and low intensity black light radiation or simulated solar radiation as excitation source. *Journal of Hazardous Materials*, 163: 756-760, (2009).
- Peralta-Zamora, P. Demoraes, S.G. Pelegrini, R. Freire, M. Reyes, J. Mansilla, H. Duran, N. Evaluation of ZnO, TiO₂ and Supported ZnO on the Photoassisted Remediation of Black Liquor, Cellulose and Textile Mill Effluents *Chemosphere*, 36, pp. 2119-2133, 1998.

- Qaradawi, S.A. Salman, S.R. Photocatalytic Degradation of Methyl Orange as a Model Compound. *Journal of Photochemistry and Photobiology A: Chem.*, 148, pp. 161–168, 2002.
- Ranjith G. Nair, Jetendra Kumar Roy, S.K. Samdarshi, A.K. Mukherjee, Enhanced visible light photocatalytic disinfection of Gram negative, pathogenic Escherichia coli bacteria with Ag/TiO₂ nanoparticles, *Colloids and Surfaces B: Biointerfaces* 86: 7–13, 2011.
- Rao, C. N. R. and Govindaraj, A. In Nanotubes and Nanowires, H. Kroto, P. O'Brien, and H. Craighead, Eds., The RSC Nanoscience and Nanotechnology Series, *Royal Society of Chemistry*, London, UK, 2005.
- Romero, M., Martín-Márquez, J. & Rincón, J. Ma., Kinetic of mullite formation from a porcelain stoneware body for tiles production, *Journal of the European Ceramic Society.*, 26, 1647-1652, 2006.
- Ryan KJ, Ray CG, *Sherris Medical Microbiology (4th ed.)*. McGraw Hill. pp. 362–8, 2004.
- Sánchez, M. J. Gamero, P. and Cortés, D. Bioactivity Assessment of Zsm-5 Type Zeolite Functionalized with Silver or Zinc, *Materials Letters*, **74**, 250-253, 2012.
- Serpone N, Salinaro A, Emeline AV, Horikoshi S, Hidaka H, Zhao J. *Journal of Photochemical and Photobiological Sciences*; 1(12):970-81, 2003.
- Seven, O, B. Dindar, S. Aydemir, D. Metin, M.A. Ozinel and S. Icli, “Solar photocatalytic disinfection of a group of bacteria and fungi aqueous suspensions with TiO₂, ZnO and Sahara desert dust”, *Journal of Photochemistry and Photobiology. A.* 165:103–107. 94, 2004.
- Shannon, M. A., Bohn P.W, Elimelech .M, Georqiadis J.G, Marinas B.J, Mayes A.M. *Nature* 452, 301–310, 2008.
- Sharma, P. Sreenivas, K. and Rao, K. V. “Analysis of ultraviolet photoconductivity in ZnO films prepared by unbalanced magnetron sputtering,” *Journal of Applied Physics*, vol. 93, no. 7, pp. 3963–3970, 2003.
- Sihem Helali, Maria Inmaculada Polo-López, Pilar Fernández-Ibáñez, Bunsho Ohtani, Fumiaki Amano, Sixto Malato, Chantal Guillard. Solar photocatalysis: A green technology for *E. coli* contaminated water disinfection. Effect of concentration and different types of suspended catalyst. *Journal of Photochemistry and Photobiology A: Chemistry*, 276: 31–40, 2014.

- Sonuparlak, B. Sarikaya, M. Aksay, I. Spinel phase formation during 980_C exothermic reaction in the kaolinite-to-mullite reaction series, *Journal of the American Ceramic Society*. 70: 837-842, 1987.
- Suresh P, Micahel S, Nicholas N, Miguel, Athanassios G. K., Patrick S.M., Jeremy W.J., Anthony B, Kevin O, Mohammad H. E, and Dionysios D. D A Review on the Visible Light Active Titanium dioxide Photocatalysts for Environmental Applications. 125: 331-349, 2012.
- Tam, K. H. Djurišić, A. B. Chan, C. M. N. Xi, Y. Y. Tse, C. W. Leung, Y. H. Chan, W. K. Leung, F. C. C. and Au, D. W. T. Antibacterial Activity of ZnO Nanorods Prepared by a Hydrothermal Method, *Thin Solid Films*, 516(8), 6167-6174, 2011.
- Tankhiwale, R. and Bajpai, S. K. Preparation Characterization and Antibacterial Applications of Zno-Nanoparticles Coated Polyethylene Films for Food Packaging, *Colloids and Surfaces B: Biointerfaces*, 90: 16-20, 2010.
- Tarvornpanich, T., Souza, G. P. & Lee, W. E., Microstructural evolution in claybased ceramics I: Single components and binary mixtures of clay, flux and quartz filler, *Journal of the American Ceramic Society*., 91, 2264-2271, 2008.
- Tarvornpanich, T., Souza, G. P. & Lee, W. E., Microstructural evolution in clay based their toxicity to *Escherichia coli*. *Environmental Pollution*; 173:97–102, 2013.
- Tarnkamol .T, Guilherme P.S, William E.L. Ceramics II: Ternary and quaternary mixtures of clay, flux and quartz filler, *Journal of the American Ceramic Society*, , 91, 2272-2280, 2008.
- Tayel, A. El-Tras, W. F. Moussa, SH. El-Baz, A. F. Mahrous, H. Salem, M. F. Brimer, L. “Antibacterial Action of Zinc Oxide Nanoparticles Against Foodborne Pathogens”, *Journal of Food Safety*, 31, 211–218, 2011.
- Tokumoto, M. S. Briois, V.Santilli, C. V. and Pulcinelli, S. H. “Preparation of ZnO nanoparticles: structural study of the molecular precursor,” *Journal of Sol-Gel Science and Technology*, vol. 26, no. 1–3, pp. 547–551, 2003.
- Topoglidis,E. Cass, A. E. G. O'Regan, B. and Durrant, J.R. “Immobilization and bioelectrochemistry of proteins on nanoporous TiO₂ and ZnO films,” *Journal of Electroanalytical Chemistry*, vol. 517, no. 1-2, pp. 20–27, 2001.
- Tortora, G.A.*Microbiology: An Introduction*(9th ed.). Pearson. pp. 323–324, 2008.
- Tucci, A., Esposito, L., Malmusi, L. & Rambaldi, E., New body mixes for porcelain stoneware tiles with improved mechanical characteristics, *Journal of the European Ceramic Society*., 27, 1875-1881, 2007.

- Vineetha, M.N Manickam Matheswaran, K.N. Sheeba. Photocatalytic colour and COD removal in the distillery effluent by solar radiation. *Journal of Solar Energy* 91 368-373, 2013.
- Vineetha, M.N. Manickam Matheswaran, Sheeba, K.N. Photocatalytic colour and COD removal in the distillery effluent by solar radiation. *Journal of Solar energy* vol 91, 368–373, 2013.
- Wang, C. X.M. Wang, B.Q. Xu, J.C. Zhao, B.X. Mai, P.A. Peng, G.Y. Sheng, J.M. Fu Enhanced Photocatalytic Performance of Nanosized Coupled ZnO/SnO₂ Photocatalysts for Methyl Orange Degradation *Journal of Photochemistry and Photobiology. A: Chem.*, 168, pp. 47–52, 2004.
- Wang, Z. L. “Nanostructures of zinc oxide,” *Materials Today*, vol. 7, no. 6, pp. 26–33, 2004.
- Wanjun Wang, Ying Yu, Taicheng Ans, Guiying Li, Ho Yin Yip, Jimmy C. Yu, Po Keung Wong. Visible-Light-Driven Photocatalytic Inactivation of *E. coli* K-12 by Bismuth Vanadate Nanotubes: Bactericidal Performance and Mechanism. *Environmental Science and Technology*. 46 (8), pp 4599–4606, 2012.
- Zhai, H. J. Wu, W. H. Lu, F. Wang, H.S. and Wang, C. “Effects of ammonia and cetyltrimethylammonium bromide (CTAB) on morphologies of ZnO nano- and micromaterials under solvothermal process,” *Materials Chemistry and Physics*, vol. 112, no. 3, pp. 1024–1028, 2008.
- Zhang D. H., Xue, Z. Y. and Wang, Q. P. “Formation of ZnO nanoparticles by the reaction of zinc metal with aliphatic alcohols,” *Journal of Physics D*, vol. 35, no. 21, pp. 2837–2840, 2002.
- Zhou, J. Zhao, F. Wang, Y. Zhang, Y. and Yang, L. “Size-controlled synthesis of ZnO nanoparticles and their photoluminescence properties,” *Journal of Luminescence*, vol. 122-123, no. 1-2, pp. 195–197, 2007.

APPENDIX A

SYNTHESIS OF ZnO/MULLITE PHOTOCATALYST CALCULATIONS

Calculation for percentage quantity of ZnO/Mullite synthesized from the precursors (ZnCO_3 and $\text{Al}_2\text{Si}_2\text{O}_5(\text{OH})_4$) is presented below.

Basis 50g of ZnO/Mullite

ZnO	(A-1)	Kaolinite
$\frac{10}{100} \times 50 = 5g$		$\frac{90}{100} \times 50 = 45g$
$\frac{20}{100} \times 50 = 10g$		$\frac{80}{100} \times 50 = 40g$
$\frac{30}{100} \times 50 = 15g$		$\frac{70}{100} \times 50 = 35g$
$\frac{40}{100} \times 50 = 20g$		$\frac{60}{100} \times 50 = 30g$
$\frac{50}{100} \times 50 = 25g$		$\frac{50}{100} \times 50 = 25g$

The balance equation is:



Heat

Molar mass (g/mol) of each element are:

Zn=65, O=16, C=12

Material balance over reaction A-1

To produce 5g, 10g, 15g, 20g, 25g of Zinc oxide (ZnO)

Molar mass of ZnO = 81.4g/mol

Molar mass of ZnCO_3 = 125.4g/mol

The amount of ZnCO₃ required to produce 5g, 10g, 15g, 20g, of ZnO is calculated below;

$$\text{Mass of ZnCO}_3 \text{ required (x)} = \frac{125.4 \times y}{81.4}$$

In summary,

To produce ZnO/Mullite in the proportion illustrated in A-1 the following materials are charged in the furnace at 1200⁰C

ZnCO ₃ (g)	Kaolinite (g)
7.70	45
15.41	40
23.11	35
30.81	30
38.51	25

APPENDIX B

CRYSTALLINE SIZE DETERMINATION FROM XRD DATA

The crystal sizes were determined using Scherer's equation, $D = \frac{K\lambda}{\beta \cos\theta}$ from data obtained from XRD analysis. For the samples under discussion, $K=0.89$, $\lambda=0.1540$ nm and $\beta = (\Theta_2 - \Theta_1) \frac{\pi}{180}$

Where, D = particle size, nm

$$\lambda=1.54\text{\AA}$$

β = width at Full Width at Half Maximum (FWHM) in radians

2θ =Bragg angle

1. The synthesized Mullite;

$$\text{At } 2\theta = 23.81^\circ, \Theta_1 = 23.48^\circ, \Theta_2 = 24.14^\circ$$

$$\beta = (24.14 - 23.48) \frac{\pi}{180} = 0.01152$$

$$D = \frac{K\lambda}{\beta \cos\theta} = \frac{0.94 \times 0.1542}{0.01152 \times \cos 11.91} = 12.86 \text{ nm}$$

2. 10-ZnO/Mullite

$$\text{At } 2\theta = 34.11^\circ, \Theta_1 = 33.96^\circ, \Theta_2 = 34.26^\circ$$

$$\beta = (34.26 - 33.96) \frac{\pi}{180} = 0.005236$$

$$D = \frac{K\lambda}{\beta \cos\theta} = \frac{0.94 \times 0.1542}{0.005236 \times \cos 17.06} = 28.96 \text{ nm}$$

3. 20-ZnO/Mullite

$$\text{At } 2\theta = 34.26^\circ, \Theta_1 = 34.15^\circ, \Theta_2 = 34.26^\circ$$

$$\beta = (34.26 - 34.15) \frac{\pi}{180} = 0.004014$$

$$D = \frac{K\lambda}{\beta \cos \theta} = \frac{0.94 \times 0.1542}{0.004014 \times \cos 17.13} = 37.79 \text{ nm}$$

4. ZnO

$$\text{At } 2\theta = 33.76^\circ, \theta_1 = 33.68^\circ, \theta_2 = 33.84^\circ$$

$$\beta = (33.84 - 33.68) \frac{\pi}{180} = 0.002793$$

$$D = \frac{K\lambda}{\beta \cos \theta} = \frac{0.94 \times 0.1542}{0.002793 \times \cos 16.88} = 54.23 \text{ nm}$$

APPENDIX C

SURFACE AREA DETERMINATION USING SEAR'S METHOD

The specific surface areas (SSA) of the samples were determined using Sear's method according to the equation $S \text{ (m}^2\text{/g)} = 32V - 25$

1. ZnO $32 \times 3.48 - 25 = 86.2\text{m}^2/\text{g}$

2. Mullite $32 \times 7.10 - 25 = 202.2\text{m}^2/\text{g}$

3. 10-ZnO/Mullite $32 \times 5.30 - 25 = 144.6\text{m}^2/\text{g}$

$$32 \times 4.10 - 25 = 106.2\text{m}^2/\text{g}$$

4. 20-ZnO/Mullite

5. 30-ZnO/Mullite $32 \times 5.40 - 25 = 147.8\text{m}^2/\text{g}$

6. 40-ZnO/Mullite $32 \times 3.80 - 25 = 96.6\text{m}^2/\text{g}$

7. 50-ZnO/Mullite $32 \times 3.65 - 25 = 91.7\text{m}^2/\text{g}$

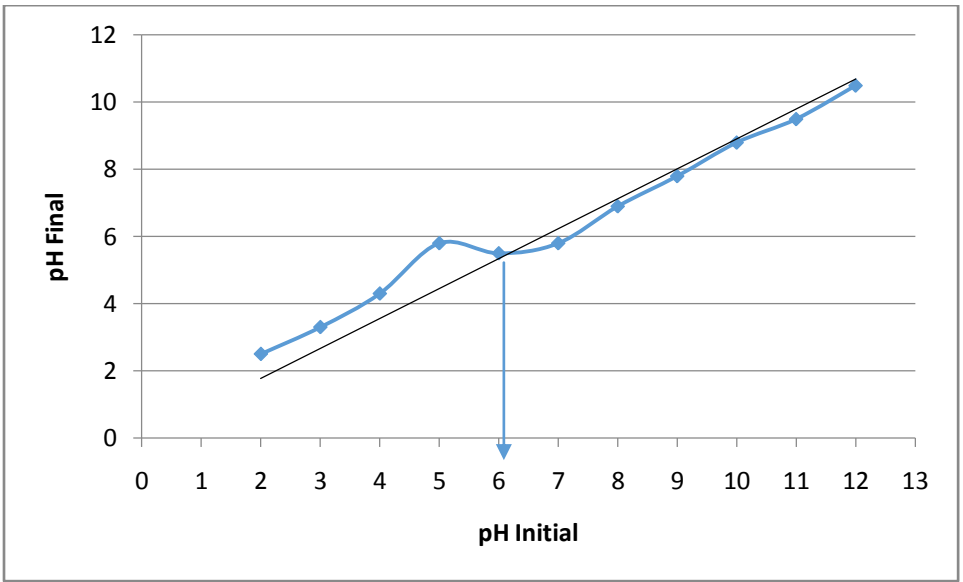
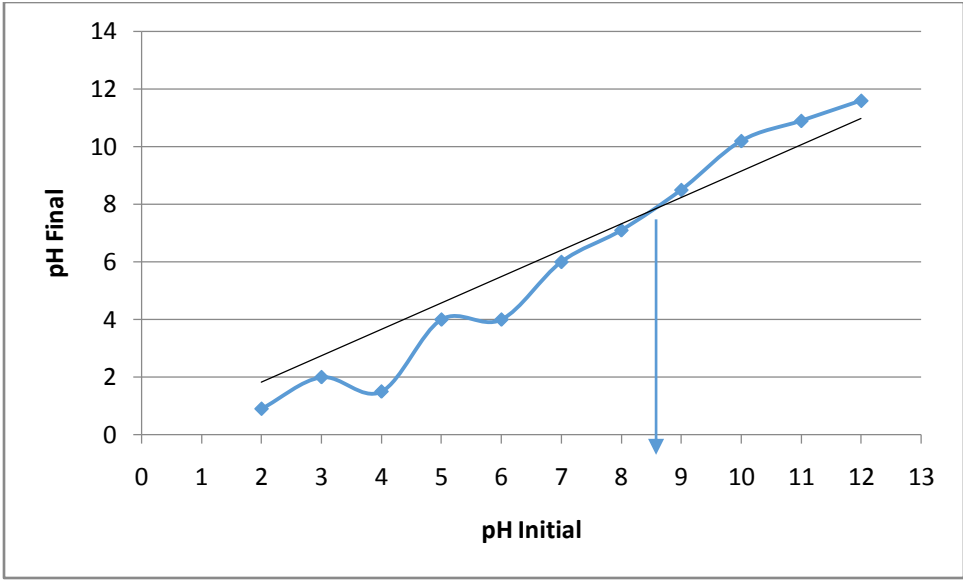
APPENDIX D

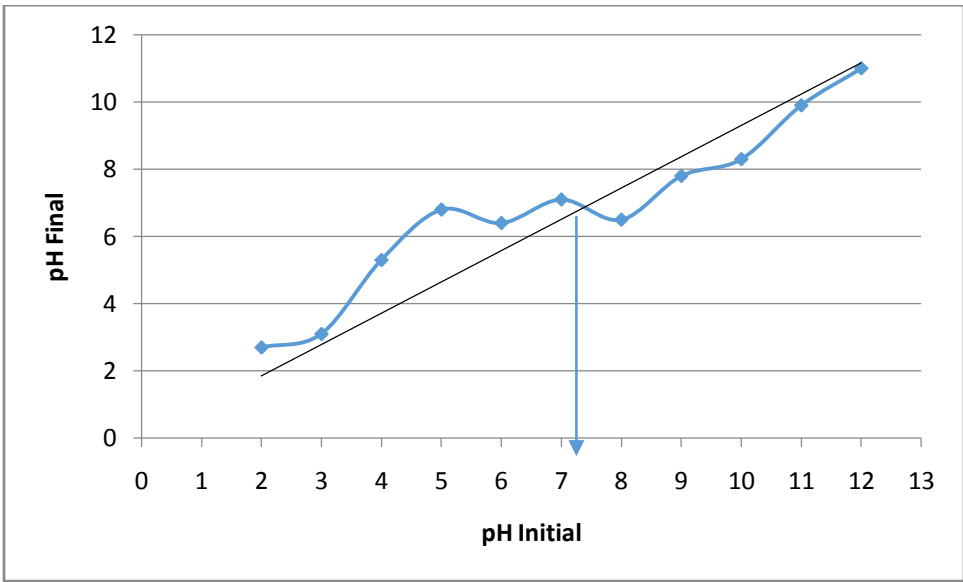
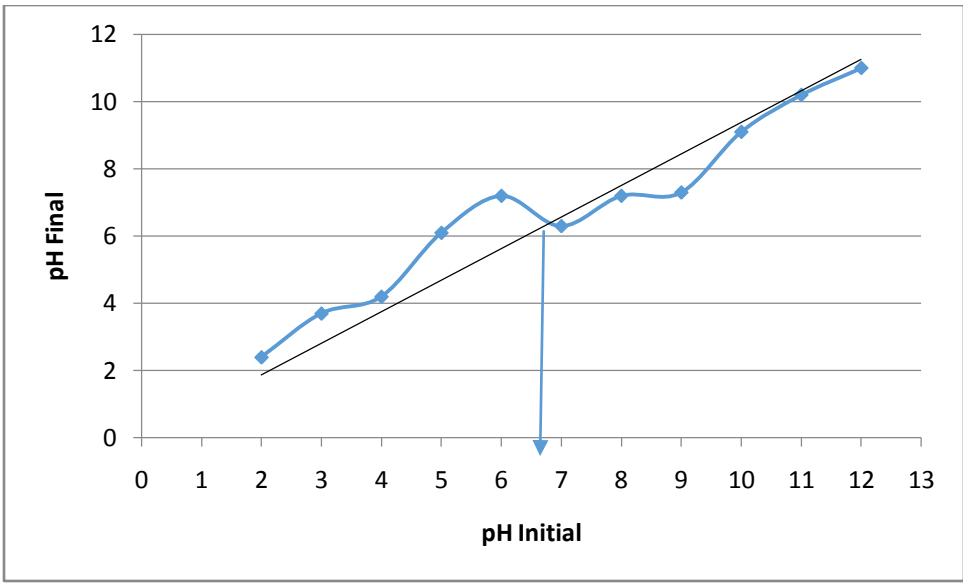
DETERMINATION OF pH AT POINT OF ZERO CHARGE USING DRIFT

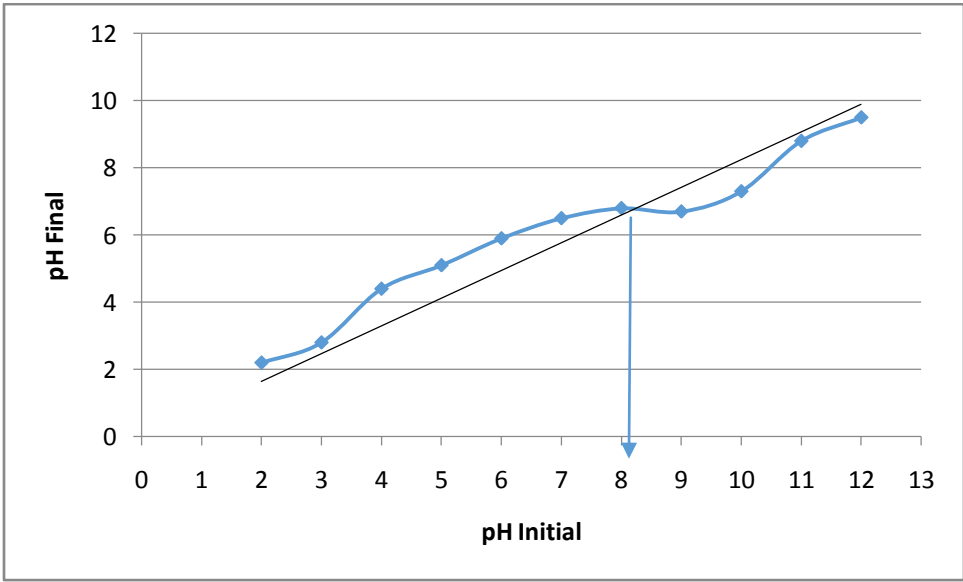
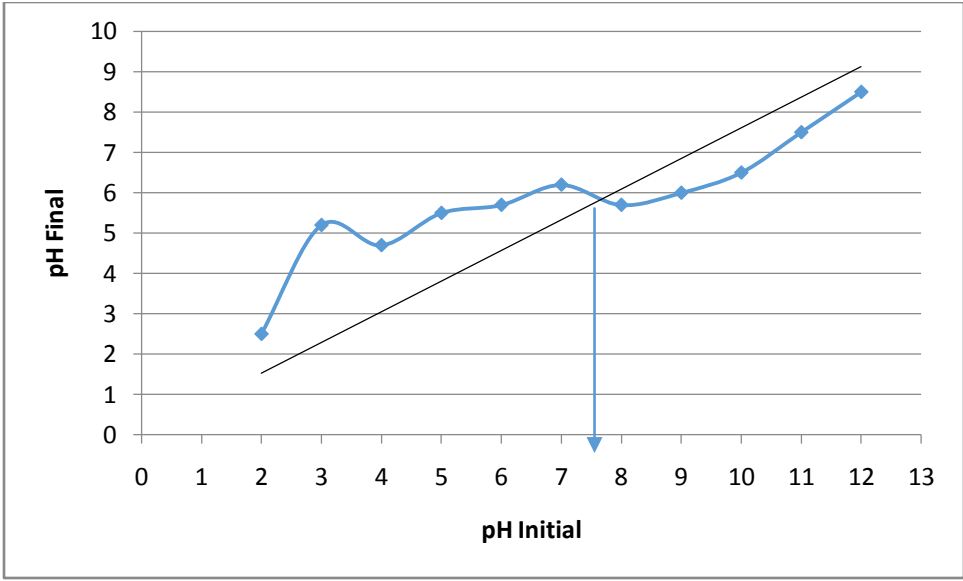
METHOD

Table D: pH values ($\text{pH}_{\text{Initial}}$ and pH_{Final}) for the photocatalysts

	ZnO	10-ZnO/M	20-ZnO/M	30-ZnO/M	40-ZnO/M	50-ZnO/M
$\text{pH}_{\text{Initial}}$	pH_{Final}	pH_{Final}	pH_{Final}	pH_{Final}	pH_{Final}	pH_{Final}
2	0.9	2.5	2.4	2.7	2.5	2.2
3	2.0	3.3	3.7	3.1	5.2	2.8
4	1.5	4.3	4.2	5.3	4.7	4.4
5	4.0	5.8	6.1	6.8	5.5	5.1
6	4.0	5.5	7.2	6.4	5.7	5.9
7	6.0	5.8	6.3	7.1	6.2	6.5
8	7.1	6.9	7.2	6.5	5.7	6.8
9	8.5	7.8	7.3	7.8	6.0	6.7
10	10.2	8.8	9.1	8.3	6.5	7.3
11	10.9	9.5	10.2	9.9	7.5	8.8
12	11.6	10.5	11	11	8.5	9.5







APPENDIX E

PRELIMINARY PHOTOCATALYTIC ACTIVITY OF THE SYNTHESIZED ZnO AND ZnO/Mullite PHOTOCATALYSTS

It should be noted that at low concentration of the pollutants, the absorbance value (A) is equal to the concentration according to Beer- Lambert's law, since the parameters ϵ and L are constants. Therefore, Absorbance (A) = Concentration (C)

$$A = \log_{10} (I/I_0) = \epsilon \cdot C \cdot L \quad \text{E-1}$$

Photocatalytic Degradation of Methylene Blue (MB)

Initial concentration of methylene blue (MB) = 10mg/L

Initial absorbance value of methylene blue (MB) = 1.412

Maximum wavelength (λ_{max}) for MB absorption = 665nm

Catalyst dosage = 0.1g/100ml of solution

Source of light = Visible light irradiation

Dark absorption = 60 minutes

Initial concentration at time zero (t = 0) using ZnO is: $C_0 = 1.292$

Initial concentration at time zero (t = 0) using 10-ZnO/mullite is: $C_0 = 1.240$

Initial concentration at time zero (t = 0) using 20-ZnO/mullite is: $C_0 = 1.201$

Initial concentration at time zero (t =0) using 30-ZnO/mullite is: $C_0 = 1.170$

Initial concentration at time zero (t =0) using 40-ZnO/mullite is: $C_0 = 1.130$

Initial concentration at time zero (t =0) using 50-ZnO/mullite is: $C_0 = 1.120$

$$\text{Degradation (\%)} = \frac{C_0 - C_t}{C_0} \times 100\%. \quad \text{E-2}$$

Table E2: % degradation for photocatalytic degradation of MB using the synthesized photocatalysts

Time (min)	ZnO	10- ZnO/mullite	20- ZnO/mullite	30- ZnO/mullite	40- ZnO/mullite	50- ZnO/mullite
0	0	0	0	0	0	0
10	7.043344	3.870968	6.827644	9.316239	10.97345	15.89286
30	45.66563	15.16129	24.97918	29.05983	37.16814	44.375
45	59.52012	25.80645	33.05579	38.03419	38.93805	59.01786
60	82.97214	33.06452	34.22148	46.75214	54.86726	68.57143

Table E3: $Ln C_0/C_t$ for photocatalytic degradation of MB using the synthesized photocatalysts

Time (min)	ZnO	10- ZnO/mullite	20- ZnO/mullite	30- ZnO/mullite	40- ZnO/mullite	50- ZnO/mullite
0	0	0	0	0	0	0
10	0.073037	0.039479	0.070719	0.097792	0.116236	0.173079
20	0.159065	0.101783	0.12772	0.239299	0.282386	0.359229
30	0.610013	0.164418	0.287405	0.343333	0.464708	0.586537
45	0.904365	0.298493	0.401311	0.478587	0.493281	0.892034
60	1.770319	0.401441	0.418877	0.630213	0.795562	1.157453

Table E4: $Ln N_0/N$ for photocatalytic inactivation of *e coli* using the synthesized 30-ZnO/mullite photocatalysts

TIME (min)	Light 0.5g	Light 1.0g	Light 1.5g	Light 2.0g	Dark 0.5g	Dark 1.0g	Dark 1.5g	Dark 2.0g
0	0	0	0	0	0	0	0	0
30	4.759321	4.941642	2.351375	2.402669	0.154151	0.182322	0.126752	0.074108
60	7.179689	7.649693	4.877104	4.877104	0.370374	0.441833	0.303682	0.271934
90	10.64542	19.85577	8.34284	10.64542	1.658228	1.658228	0.518794	0.441833

PHOTOCATALYTIC INACTIVATION OF *E. COLI* AND *S. ENTERICA* USING THE SYNTHESIZED ZnO/Mullite PHOTOCATALYSTS

Table F1: *E. coli* inactivation in the dark/light using 0.5/L

ZnO			10-ZnO/Mullite		
Time	Dark	Light	Time	Dark	Light
0	4.20×10^6	4.20×10^6	0	4.20×10^6	4.20×10^6
30	2.45×10^6	3.70×10^4	30	3.70×10^6	3.90×10^5
60	1.52×10^6	1.85×10^4	60	3.30×10^6	1.30×10^3
90	1.50×10^6	0.00×10^0	90	2.10×10^6	2.00×10^2

20-ZnO/Mullite			30-ZnO/Mullite		
Time	Dark	Light	Time	Dark	Light
0	4.20×10^6	4.20×10^6	0	4.20×10^6	4.20×10^6
30	3.90×10^6	2.20×10^6	30	3.60×10^6	3.50×10^5
60	3.40×10^6	2.00×10^5	60	2.90×10^6	8.30×10^4
90	2.80×10^6	1.20×10^3	90	1.40×10^6	0.00×10^0

40-ZnO/Mullite			50-ZnO/Mullite		
Time(min)	Dark	Light	Time(min)	Dark	Light
0	4.20×10^6	4.20×10^6	0	4.20×10^6	4.20×10^6
30	4.00×10^6	3.80×10^6	30	4.10×10^6	3.90×10^6
60	3.70×10^6	1.60×10^4	60	3.90×10^6	1.30×10^4
90	3.50×10^6	3.50×10^3	90	3.80×10^6	5.00×10^3

Table F2: *E. coli* inactivation in the dark/light using 1g/L

Time	ZnO	
	Dark	Light
0	4.20×10^6	4.20×10^6
30	2.40×10^6	3.50×10^3
60	1.49×10^6	1.42×10^3
90	4.00×10^5	0.00×10^0

Time	10-ZnO/mullite	
	Dark	Light
0	4.20×10^6	4.20×10^6
30	3.60×10^6	3.70×10^4
60	3.10×10^6	1.20×10^3
90	2.00×10^6	1.50×10^2

Time	20-ZnO/mullite	
	Dark	Light
0	4.20×10^6	4.20×10^6
30	3.70×10^6	4.10×10^4
60	3.20×10^6	2.00×10^4
90	2.50×10^6	2.20×10^2

Time	30-ZnO/mullite	
	Dark	Light
0	4.20×10^6	4.20×10^6
30	3.50×10^6	3.40×10^4
60	2.70×10^6	2.00×10^4
90	8.00×10^5	0.00×10^0

Time	40-ZnO/mullite	
	Dark	Light
0	4.20×10^6	4.20×10^6
30	3.90×10^6	4.10×10^4
60	3.40×10^6	2.50×10^4
90	3.20×10^6	3.00×10^2

Time	50-ZnO/mullite	
	Dark	Light
0	4.20×10^6	4.20×10^6
30	4.00×10^6	5.20×10^4
60	3.70×10^6	3.05×10^4
90	3.50×10^6	3.80×10^2

Table F3: *E.coli* inactivation in the dark/light using 1.5g/L

Time	ZnO	
	Dark	Light
0	4.20×10^6	4.20×10^6
30	3.10×10^6	3.70×10^4
60	1.80×10^6	1.13×10^4
90	1.30×10^6	2.00×10^2

Time	10-ZnO/mullite	
	Dark	Light
0	4.20×10^6	4.20×10^6
30	3.90×10^6	3.80×10^5
60	3.60×10^6	5.00×10^4
90	2.90×10^6	1.40×10^4

Time	20-ZnO/mullite	
	Dark	Light
0	4.20×10^6	4.20×10^6
30	4.00×10^6	4.00×10^5
60	3.70×10^6	8.00×10^4
90	3.30×10^6	8.00×10^3

Time	30-ZnO/mullite	
	Dark	Light
0	4.20×10^6	4.20×10^6
30	3.70×10^6	3.60×10^5
60	3.10×10^6	3.20×10^4
90	2.50×10^6	1.00×10^3

Time	40-ZnO/mullite	
	Dark	Light
0	4.20×10^6	4.20×10^6
30	4.10×10^6	4.10×10^5
60	3.80×10^6	1.20×10^5
90	3.50×10^6	8.00×10^4

Time	50-ZnO/mullite	
	Dark	Light
0	4.20×10^6	4.20×10^6
30	4.10×10^6	2.00×10^6
60	3.90×10^6	2.00×10^5
90	3.60×10^6	2.10×10^4

Table F4: *E.coli* inactivation in the dark/light using 2g/L

ZnO		
Time	Dark	Light
0	4.20×10^6	4.20×10^6
30	3.60×10^6	3.80×10^4
60	2.00×10^6	1.13×10^4
90	1.40×10^6	2.00×10^2

10-ZnO/mullite		
Time (min)	Dark	Light
0	4.20×10^6	4.20×10^6
30	4.00×10^6	3.90×10^5
60	3.80×10^6	2.00×10^5
90	3.20×10^6	1.80×10^4

20-ZnO/mullite		
Time (min)	Dark	Light
0	4.20×10^6	4.20×10^6
30	4.10×10^6	4.10×10^5
60	3.80×10^6	3.00×10^5
90	3.50×10^6	2.50×10^4

30-ZnO/mullite		
Time (min)	Dark	Light
0	4.20×10^6	4.20×10^6
30	3.90×10^6	3.80×10^5
60	3.20×10^6	3.20×10^4
90	2.70×10^6	1.05×10^3

40-ZnO/mullite		
Time (min)	Dark	Light
0	4.20×10^6	4.20×10^6
30	4.10×10^6	4.10×10^6
60	3.80×10^6	4.00×10^6
90	3.70×10^6	3.20×10^6

50-ZnO/mullite		
Time (min)	Dark	Light
0	4.20×10^6	4.20×10^6
30	4.10×10^6	4.10×10^6
60	4.00×10^6	4.10×10^5
90	3.70×10^6	4.00×10^4

Table F: *Salmonellai* inactivation in the dark/light using 0.5g/L and 1g/L

Time (min)	10-ZnO/mullite	
	Dark	Light
0	4.20×10^6	4.20×10^6
30	3.60×10^6	3.70×10^5
60	3.10×10^6	1.00×10^5
90	1.90×10^6	1.80×10^2

Time (min)	10-ZnO/mullite	
	Dark	Light
0	4.20×10^6	4.20×10^6
30	3.20×10^6	3.50×10^4
60	2.80×10^6	5.0×10^4
90	1.60×10^6	1.00×10^2

Time (min)	30-ZnO/mullite	
	Dark	Light
0	4.20×10^6	4.20×10^6
30	3.50×10^6	3.20×10^5
60	2.70×10^6	7.00×10^4
90	9.00×10^3	0.00×10^0

Time (min)	30-ZnO/mullite	
	Dark	Light
0	4.20×10^6	4.20×10^6
30	3.10×10^6	2.90×10^4
60	2.30×10^6	1.00×10^4
90	4.00×10^5	0.00×10^0

APPENDIX G

COD Determination of Zaria dam raw water solution under photocatalysis.

$$COD = \frac{(a - b) \times c \times 8000}{Volume\ of\ sample\ used}$$

Where : a- volume for blank = 8.50

b- volume for sample

c- volume of normality = 0.25N

volume of samples = 20ml

COD of raw water = 750mg/L

Photocatalyst	COD (dark)	COD (light)	% COD removal (Dark)	% COD removal (light)
ZnO	730	640	2.67	14.67
10-ZnO/mullite	720	630	4.00	16.00
20-ZnO/mullite	710	617	5.33	17.73
30-ZnO/mullite	690	600	8.00	20.00
40-ZnO/mullite	670	350	10.67	53.33
50-ZnO/mullite	640	270	14.67	64.00
Mullite	745	739	0.67	1.47